Universidad Zaragoza
1542

Trabajo Fin de Máster

Caracterización in vitro e in silico de estructuras open-cell para hueso trabecular. Prevención de la fractura osteoporótica

In vitro and in silico characterization of open-cell structures for trabecular bone. Osteoporotic fracture prevention

Autor/es

Samuel Jesús Ramos Infante

Director/es

Mª Ángeles Pérez Ansón

Escuela de Ingeniería y Arquitectura

2016

TRABAJOS DE FIN DE GRADO / FIN DE MÁSTER

Escuela de Ingeniería y Arquitectura Universidad Zaragoza

DECLARACIÓN DE AUTORÍA Y ORIGINALIDAD

(Este documento debe acompañar al Trabajo Fin de Grado (TFG)/Trabajo Fin de Máster (TFM) cuando sea depositado para su evaluación).

D./Dª. SAMUEL JESÚS RAMOS INFANTE,

con nº de DNI 44745848-S en aplicación de lo dispuesto en el art. 14 (Derechos de autor) del Acuerdo de 11 de septiembre de 2014, del Consejo de Gobierno, por el que se aprueba el Reglamento de los TFG y TFM de la Universidad de Zaragoza,

Declaro que el presente Trabajo de Fin de (Grado/Máster) MÁSTER, (Título del Trabajo) CARACTERIZACIÓN IN VITRO E IN SILICO DE ESTRUCTURAS OPEN-CELL PARA HUESO TRABECULAR. PREVENCIÓN DE LA FRACTURA OSTEOPORÓTICA,

es de mi autoría y es original, no habiéndose utilizado fuente sin ser citada debidamente.

Zaragoza, 20 DE SEPTIEMBRE DE 2016

Fdo: SAMUEL JESÚS RAMOS INFANTE

Acknowledgements

It is my pleasure to gratefully thank all the people that made this TFM possible; they are all key participants of this work.

Firstly, I would like to thank you my parents, Luis and Fabiola, for being near me and they not only gave me life, but also fill it with all the affection, support and love one could wish for. They have always encouraged and supported me to do my best in all matters of life. Thank you.

Secondly, I would like to express my gratitude to Dra. Mª Ángeles Pérez Ansón. It is difficult to overstate my gratitude to Mª Ángeles for being so involved in my TFM and for all the support I have received from her. I would like to thank you so much for trust in me since the beginning of my Master´s Degree and help me in difficult moments of my TFM. Thank you.

Also, I can´t forget Dr. Alejandro Yánez Santana and Dr. Óscar Martel Fuentes for his continuous motivation since I started in biomedical engineering in University of Las Palmas de Gran Canaria. Thank you.

Furthermore, it is a pleasure to thank so much Materialise Company for awarding me with the EMEA Second Prize of the Mimics Innovation Awards 2016.

Finally, the authors gratefully acknowledge the support of the Spanish Ministry of Economy and Competitiveness through research project DPI2014-53401-C2-1-R.

Caracterización in vitro e in silico de estructuras open-cell para hueso trabecular. Prevención de la fractura osteoporótica

Resumen

Se espera que la osteoporosis sea partícipe de más de 9 millones de nuevas fracturas en todo el mundo, ya que es una de las enfermedades con mayor índice de impacto entre la población de los países desarrollados. Se define como una enfermedad ósea caracterizada por la pérdida de masa ósea con un aumento de la fragilidad y susceptibilidad a la fractura. Se sabe, además, que el hueso trabecular interviene, en gran medida, en las fracturas de cadera osteoporóticas. De hecho, numerosos estudios han intentado resolver las limitaciones derivadas de su morfología en la predicción del fallo óseo. Un tratamiento preventivo alternativo para reducir el riesgo de fractura osteoporótica incluye la inyección de cemento óseo (PMMA) en el fémur osteoporótico.

Por lo tanto, el objetivo final de este TFM es conocer más los mecanismos de fallo asociados a la osteoporosis y poder usar los resultados obtenidos para ayudar a prevenir las fracturas osteoporóticas introduciendo cemento.

Para alcanzar este objetivo, en este TFM se utilizan métodos experimentales y computacionales basados en el procesado de imagen con el fin de estimar el módulo elástico y las porosidades de diferentes estructuras open-cell (Sawbones, Malmö, Sweden). Por un lado, se caracterizaron experimentalmente tres tipos de estructuras de diferente densidad. Por otro lado, parte de esas estructuras se escanearon en un microCT, y a partir de las imágenes de tomografía computerizada se pudo predecir el módulo elástico, desarrollando para ello modelos de elementos finitos basados en elementos voxels y tetraedros. Se llevó a cabo una reconstrucción 3D usando MIMICs y 3-MATIC (Materialise NV, Lovaina, Bélgica), lo que permitió ejecutar análisis basados en el método de los elementos finitos en ABAQUS (Dassault Systèmes Simulia Corp., Suresnes Francia). Seguidamente, se llevó a cabo un análisis comparativo entre las tipologías de mallas empleadas (mallas basadas en tetraedros lineales y cuadráticos, así como mallas de voxels), de los resultados computacionales con los experimentales,

así como con los datos de propiedades mecánicas dados por el fabricante de las estructuras. Así, se obtuvieron diferencias importantes tanto en el módulo elástico como en las porosidades asociadas. Se observó que los elementos basados en tetraedros lineales presentaban mayores correlaciones en aquellos especímenes con menor porosidad. Por el contrario, los elementos cuadráticos representaban de una manera más adecuada aquellos especímenes con mayores porosidades.

Además se ha desarrollado un modelo de difusión de cemento basado en la Teoría del Movimiento Aleatorio para predecir la difusión del mismo en un medio poroso como es el hueso trabecular osteoporótico. En los resultados obtenidos, se ha observado como la inyección de cemento mejora las propiedades mecánicas de las estructuras porosas.

Palabras clave: MIMICS, estructuras open-cell, tetraedros, voxels, difusión

In vitro and in silico characterization of open-cell structures for trabecular bone. Osteoporotic fracture prevention

Abstract

Osteoporosis is a major health concern in virtually all developed countries with up to 9 million new osteoporotic fractures expected annually worldwide. It is defined as a systemic skeletal disease characterized by low bone mass, with a consequent increase in bone fragility and susceptibility to fracture. As trabecular bone is mainly involved in osteoporotic hip fractures, numerous studies have tried to solve the limitations of quantitative morphometry in the prediction of bone failure. Augmentation of osteoporotic femur using PMMA bone cement to prevent or reduce the risk of fracture has been suggested to be an alternative preventive treatment.

The main goal of this TFM is to know more about the failure mechanisms associated to osteoporosis and to be able to use these results to help to prevent osteoporotic fractures injecting bone cement.

Therefore, to achieve this goal, in this TFM it is used experimental and image-based computational methods to estimate elastic modulus and porosities of different open-cell structures (Sawbones, Malmö, Sweden). On one hand, three different open-cell structures with different porosity were characterized. On the other hand, some open-cell structures were scanned using a Microcomputed Tomography System (CT), whose data was used to non-destructively predict the specimen elastic moduli developing voxel-based and tetrahedral finite element (FE) models. A 3D reconstruction was performed using MIMICs and 3-MATIC (Materialise NV, Leuven, Belgium) and finite element analyses (FEA) were run in ABAQUS (Dassault Systèmes Simulia Corp., Suresnes Frances). A comparison among different element types (linear and quadratic tetrahedrons and voxel-base meshes), experimental and computational results and computational results with data provided by Sawbones (Sawbones, Malmö, Sweden) were carried out. As a result, important differences in the elastic modulus and porosities were obtained. Linear tetrahedral elements showed better correlations in specimens with

higher volume fractions. In contrast, specimens with low volume fractions showed better correlations with quadratic tetrahedral elements.

The development of a cement diffusion model based on the random-walk theory will help us to predict the diffusion of the cement through the porous medium of osteoporotic cancellous bone, increasing the mechanical properties. It should be pointed out that cement injection will increase the mechanical properties of open-cell structures.

Keywords: MIMICS, open-cell structures, voxel mesh, tetrahedral mesh, diffusion

Contents

Figure contents

Table contents

Chapter 1
Introduction

1.1 Clinical scenario: Trabecular bone and osteoporosis

1.1.1 Bone tissue

Bone has an important combination of physical properties, showing a very high resistance to traction and compression [Fawcett, 1994]. At the same time it presents certain elasticity and the advantage of being relatively light material. At all organization levels, from the macroscopic to the submicroscopic structure of bones, their constitution ensures the maximum resistance with reduced material and lowest weight. [Alberich, 2010]

The bone mineral substance has two main functions: a biomechanical one (stability of the skeleton) and a metabolic one (reservoir for many ions, control of mineral homeostasis). [Boivin and Meunier, 2003]

At the macroscopic scale, bone is composed of cortical (compact) bone, forming a hard outer layer, and trabecular (spongy) bone, filling the interior spaces and ends of long bones [Olszta et al., 2007]. In combination with cortical bone, trabecular bone is a major load-bearing biological tissue in human bone. It is involved in bone femur fractures and is the primary site for the insertion of orthopedic implants. [Eswaran et al., 2006]

At the submicroscopic scale, bone is a multi-phase composite material consisting of organic phase (32‑44% bone volume (BV)), inorganic phase (33‑43% BV) and water (15‑25% BV). The organic phase is composed of collagen type I (approx. 90%) and non-collagenous proteins (NCPs) (approx. 10%). The inorganic (mineral) phase is made of calcium phosphate, which is similar to hydroxyapatite (HA), $Ca_{10}(PO_4)_6(OH)_2$. The mineral phase is stiff and strong but brittle, whereas the collagen phase is soft and highly deformable. Water plays an important role in the bio-mineralization process and serves as a plasticizer, enhancing the toughness of bone. These components are arranged into a complex hierarchical structure, which makes bone stiff, strong, tough and yet lightweight. [Buehler, 2008] Five levels of hierarchical organization in bone are defined (*Figure 1*).

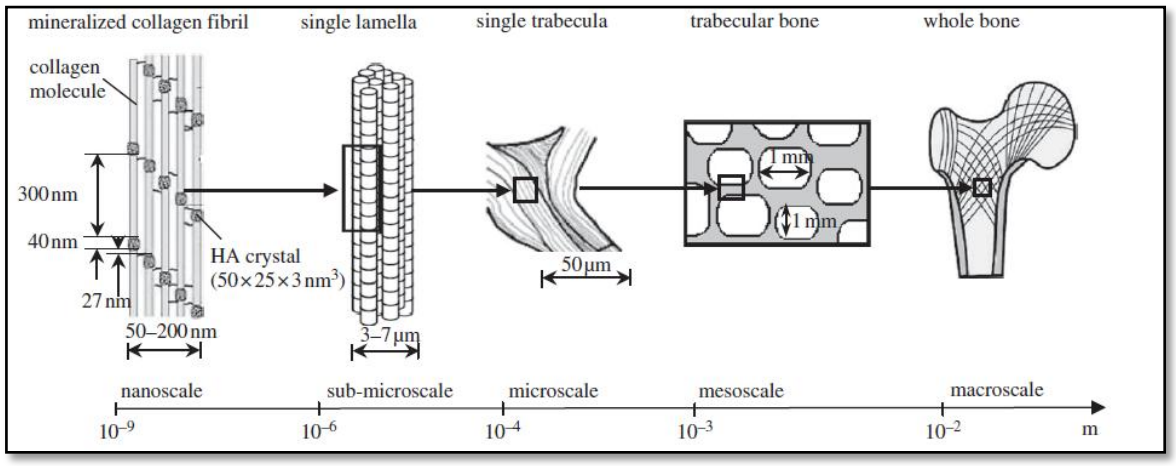

Figure 1: *Hierarchical structure of trabecular bone [Hamed et al., 2012]*

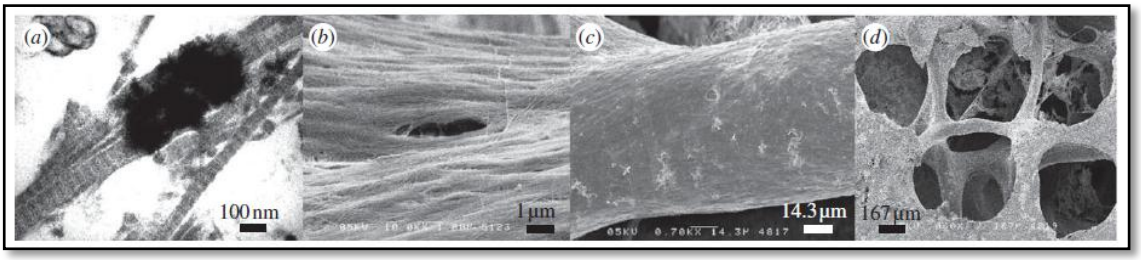

Figure 2: *Electron microscopy images of trabecular bone taken at (a) nanoscale level (10 000x), using transmission electron microscopy (TEM), showing mineralized collagen fibrils, (b) sub-microscale (1000x) showing single lamella, (c) microscale (700x) showing a trabecular strut and (d) mesoscale (20x) showing a porous cellular structure of trabecular bone, using scanning electron microscopy (SEM). [Hamed et al., 2012]*

As we can see in *Figure 1*, trabecular bone corresponds to mesoscale, ranging from hundred micrometres to several millimetres, or larger, depending on the bone size, consists of a porous network of trabeculae (*Figure 2*). The pores, typically in the order of 1 mm, are filled with bone marrow, fat and bone cells. In cortical bone, this level represents randomly arranged osteons embedded in an interstitial lamella, with some resorption cavities, all surrounded by a circumferential bone. [Hamed et al., 2012]

Bone provides the stability of the organism, harbors hematopoiesis in the bone marrow, opens up regulatory interfaces to other organs and to metabolism, and functions as a reservoir for the delivery of minerals. Bone is efficiently regenerated throughout life and shows a high capacity of scarless healing. Its strength in terms of fracture resistance results from bone mass, anatomy and microstructure and this is optimally adapted to the power and direction of mechanical forces that occur in everyday life. The sensitivity of the skeleton towards incoming mechanical forces is such that the resulting bone suffices to produce adequate fracture resistance under physiological circumstances. The musculoskeletal unit, consisting of bone, joints, ligaments, tendons and muscle translates forces into bone and orchestrates the principle of “form follows function”. [Chen et al., 2010]

Bone formation and resorption are regulated by core signaling pathways for osteoblast/osteocyte differentiation and for osteoclast recruitment, differentiation and activation. Mesenchymal progenitor cells can give rise to e.g. bone, cartilage, fat and tendon.

From its initial formation to growth, maturation and dissolution, apatite crystals interact with the water from the bone matrix. Since crystals do not grow if ions do not diffuse from the milieu, the degree of mineralization does not progress when the water content is too low. Consequently, mineralization is rarely complete and stops at about 90–95% of the expected maximum level. In young bone tissue, the water content is high and ions are constantly exchanged with apatite. Conversely, in old bone tissue, these exchanges decrease considerably.

It is generally agreed that strength of bones depends on the volume of bone matrix and the microarchitectural distribution of this volume, while the degree of mineralization of bone tissue (DMB) is almost never mentioned as a determinant of bone strength. It now has evidence that the DMB strongly influences not only the mechanical resistance of bones but also the bone mineral density (BMD) (*Figure 3*). It exists an heterogeneity in the DMB is explained by the fact that bone formation which follows bone resorption in the remodeling sequence is a multistep process: following its deposition, the new matrix begins to mineralize after about 5–10 days from the time of deposition. After full completion of the BSUs (Basic Structural Units), a phase of secondary mineralization begins. This process consists of a slow and gradual maturation of the mineral component, including an increase in the amount of crystals and/or an augmentation of crystal size toward their maximum dimensions. This secondary mineralization progressively augments the mineral content in bone matrix. At the end of the primary mineralization, mineral content represents only about 50% of the maximum degree of mineralization obtained at the end of the secondary mineralization phase. [Boivin and Meunier, 2003]

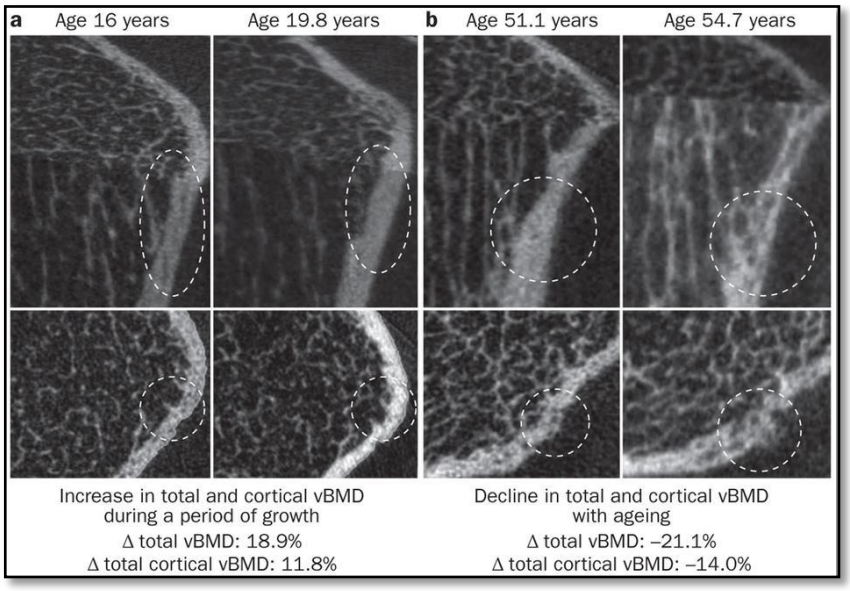

Figure 3: *Bone mass evolution with aging [González and Riancho, 2004]*

In the particular case in which rapid formation of new bone is mandatory, such as in periods of fracture curation, in skeletal growth in early childhood, or in a particular metabolic bone disorders, instead of lamellar bone, a provisional distribution of bone is formed, in which the collagen fibers are randomly oriented. Under physiologic conditions, this provisional bone is replaced after some time by lamellar bone, which has better mechanical properties. [Baron, 2003; Marks and Hermey, 1996]

After menopause, increased remodeling with a more negative bone balance in the many BMUs removes more bone rapidly from an ever-diminishing and architectural disrupted bone. [Alberich, 2010]

1.1.2 Osteoporosis

Osteoporosis is a major health concern in all developed countries with up to 9 million new osteoporotic fractures expected annually worldwide. The excess mortality rate associated with fragility fractures exceeds 20% in the first year after the fracture. In the United States, osteoporosis affects as many as 10 million individuals over the age of 50 years, with 2 million fractures occurring annually. With the aging world population, these staggering numbers are projected to double over the next 40 to 50 years with 6 million hip fractures expected to occur worldwide by 2050. [Johnell and Kanis, 2006; Kanis, 2007; Kanis et al., 2013; Odén et al., 2013] The most common osteoporotic fractures comprise vertebral fractures, fractures of the forearm (particularly Colles' fracture), hip fractures, and proximal humerus fractures. [Svedbom et al., 2013]

Osteoporosis is now recognized as one of the major public health problems facing postmenopausal women and aging individuals irrespective of gender [Riggs and Melton, 1993]. It is a syndrome of dysadaptation [Jakob et al., 2013] and conceptually defined as a systemic skeletal disease characterized by low bone mass and microarchitectural deterioration of bone tissue, with a consequent increase in bone fragility and susceptibility to fracture. Bone strength reflects the integration of two main features: bone mineral density expressed as grams of mineral per area/volume and bone quality, referring to bone architecture, turnover, damage accumulation, collagen cross-linking, and bone mineralization [Consensus development conference: diagnosis, prophylaxis and treatment of osteoporosis, 1993].

The description of osteoporosis captures the notion that low bone mass is an important component of the risk of fracture, but other abnormalities such as micro-architectural deterioration contribute to skeletal fragility. Ideally, clinical assessment of the skeleton should capture all these determinants of fracture risk, but at present the assessment of bone mass is the only aspect that can be readily measured in clinical practice (DXA), and forms the cornerstone for the general management of osteoporosis being used for diagnosis, risk prediction, and monitoring of patients on treatment.

The diagnostic criterion for osteoporosis is based on the measurement of BMD. BMD is most often described as a T-score or Z-score, both of which are units of SD. The Z-score describes the number of SDs by which the BMD in an individual differs from the mean value expected for age and sex (*Figure 4*). The T-score describes the number of SDs by which the BMD in an individual differs from the mean value expected in young healthy individuals.

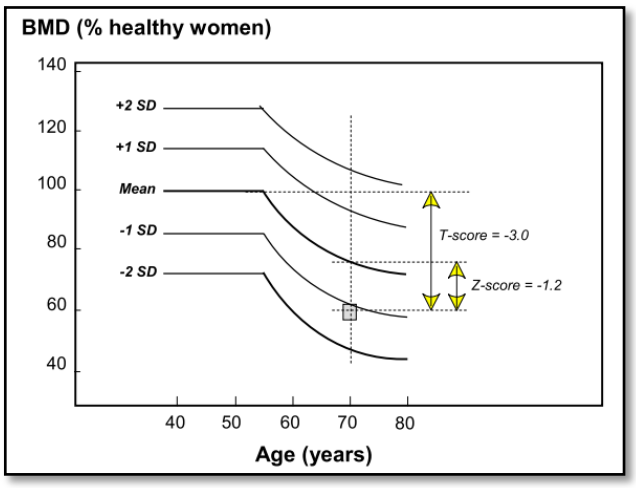

Figure 4: *Schematic diagram showing the mean BMD with SD intervals in women by age and the derivation of Z-scores and T-scores from BMD [Svedbom et al., 2013]*

The operational definition of osteoporosis is based on the T-score for BMD in women and is defined as a value for BMD 2.5 SD or more below the young female adult mean (T-score less than or equal to –2.5 SD) as shown in *Figure 5*. This threshold was originally developed for measurements of BMD at the spine, hip, or forearm. More recently, the operational definition of osteoporosis has been refined by WHO with the femoral neck as the standard measurement site and the use of an international reference standard for the calculation of the T-score.

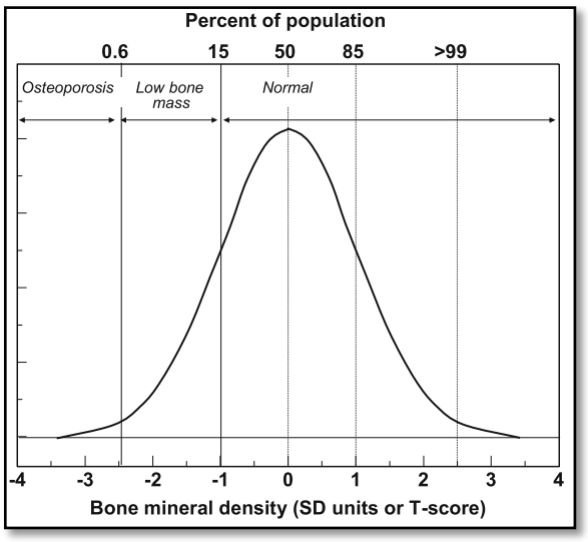

Figure 5: *The distribution of BMD in young healthy women in SD units and threshold values for osteoporosis and low bone mass [Svedbom et al., 2013]*

Osteoporosis represents a major non-communicable disease of today and is set to increase markedly in the future. There is underutilisation of the measures available to combat the disease and there is therefore a need for assessment of best practices in prevention and treatment, since the adoption of these across countries can potentially result in significant reductions in the burden of this disease. [Svedbom et al., 2013]

1.2 Motivation

1.2.1 Trabecular bone

Cancellous bone constitutes much of the volume of bone which makes up axial skeletal sites, such as the vertebrae of the spine and the proximal femur. The increased vascularity of cancellous bone compared with cortical bone means that it is more prone to drug-, endocrine- and metabolic-related effects and, therefore these skeletal sites are more risk to the bone condition osteoporosis.

The salient cancellous bone properties vary greatly as a function of its apparent density. Its elastic compressive modulus at 75% porosity is around 160 MPa, close to the human bone trabecular compressive modulus [Pioletti, 2010]. Cancellous bone is capable at the macroscopic level of large elastic–plastic behaviour, which is due to the microstructural deformations caused by the buckling/bending and rotation of the trabeculae. The other reason of course is the experimental difficulties in isolating samples of a certain size, design, orientation and of course imposing the necessary loads in a way prescribed in FT testing methods. [Cook and Zioupos, 2009]

Bone is anisotropic, meaning that its properties vary depending on the direction of loading. This is particularly difficult to handle in FEA involving cancellous bone as the trabecular struts themselves are running in different directions. Nevertheless, bone is not an isotropic material (*Figure 6*), and models that assume isotropy are inherently flawed. Moreover, bone is not linearly elastic, but rather viscoelastic. This means that the rate of loading is very important in determining the resulting stress and strain. Bone that is loaded at a higher rate will exhibit stiffer behaviour, whereas, bone loaded more slowly will appear to be less stiff. [Burr, 2016]

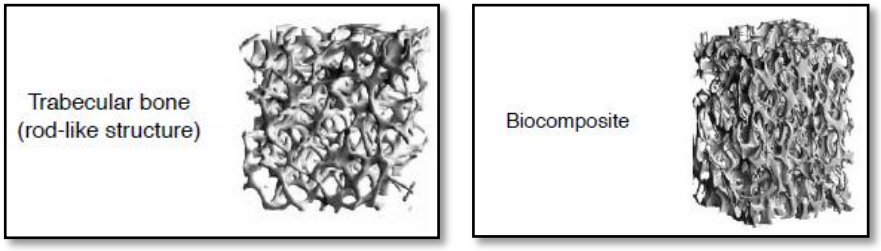

Figure 6: *Trabecular bone as an anisotropic material [Pioletti, 2010]*

The assessment and prediction of bone strength has traditionally been related to independent measures aimed at explaining the variation in stiffness and strength. However, it has also been recognized that older persons may lose bone, as expressed by a decrease in bone density, but do not develop fractures because bone mineral density, bone geometry, bone microarchitecture, and bone material properties are all contributing components which determine bone strength. [Keller, 1994; Carter and Hayes, 1977]

The limitations of quantitative morphometry in the prediction of bone failure has been demonstrated in previous studies, in which it was shown that strength of trabecular bone specimens depends on the orientation of the applied load [Bevill et al., 2009; Parkinson et al., 2012] and on local variations in the trabecular network. [Perilli et al., 2012]

It has been employed a lot of models to predict the mechanical properties of the trabecular bone, for instance, elastic behaviour of trabecular bone was studied using several different approaches, involving analytical and computational techniques. Analytical studies represented trabecular bone as a cellular solid and expressed its Young´s modulus by power law relations in terms of density [Gibson et al., 1982; Gibson, 1985; Gibson and Ashby, 1982, 1999; Gibson et al., 2010; Rajan, 1985]. Although density is a key parameter in determining properties of trabecular bone, it alone cannot fully capture the mechanical behaviour of bone. Other researchers defined a fabric tensor, which characterizes the textural or structural anisotropy of trabecular bone, and found the relationships between the elastic constants of trabecular bone and its fabric tensor and density [Kabel et al., 1999; Turner et al., 1990; Zysset, 2003]. Trabecular bone´s architecture, characterized by thickness, number and separation distance of individual trabecula as well as their three-dimensional connectivity, plays an important role in its response. Thus, high-resolution imaging techniques, such as micro-computed tomography (μCT), accounting for actual trabecular bone architecture, were used in combination with the Finite Element Method (FEM) to predict elastic moduli of trabecular bone (*Figure 7*) [Müller and Rüegsegger, 1995; Ulrich et al., 1998; Bourne et al., 2004; Harrison et al., 2008; Dobson et al., 2006; Follet et al., 2007; Pahr and Zysset, 2008].

Trabecular bone tissue failure can be considered as consisting of two stages: damage and fracture. [Taylor, 2003; Wachtel and Keaveny, 1997; O'Brien et al., 2002; Yeh and Keaveny, 2001; Gupta and Zioupos, 2008].

- **Damage:** is considered to be a loss of mechanical integrity, stiffness or strength but with the material remaining intact, that is, no new surfaces are created.
- **Fracture:** is considered to be the separation of (previously damaged) material producing new surfaces, with the separation in the structure leading to an inability to transfer load between the new surfaces. [Harrison et al., 2013]

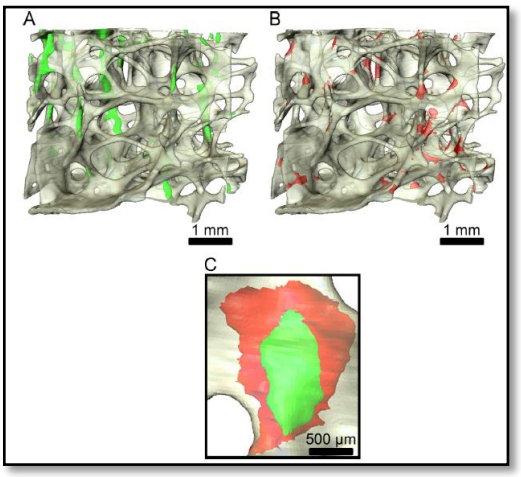

Figure 7: *A specimen of trabecular bone. (A) Highly strained tissue is indicated in green. (B) Microdamage is indicated in red. (C) Image registration was used to determine the spatial associations between microdamage and highly strained tissue [Goff et al., 2015]*

1.2.2 Femoroplasty and cement injection

Trabecular bone is mainly involved in osteoporotic hip fractures. These are costly and constitute a major health problem worldwide [Lane et al., 2000; Elffors, 1998]. Current preventive measures include hip protectors, which cause discomfort and are limited due to patient non-compliance, and a variety of drugs, limited in efficacy due to long delays in restoring bone strength, high costs, and side effects such as an increased risk of cancer [Delmas et al., 1997; Ettinger et al., 1998; Khovidhunkit and Shoback, 1999; Kannus et al., 2000]. An alternative preventive intervention is femoral augmentation-also referred to as femoroplasty-which is the process of injecting acrylic bone cement into the proximal femur to prevent osteoporotic hip fractures [Beckmann et al., 2007, 2011; Heini et al., 2004; Sutter et al., 2010a]. Femoroplasty increases the strength and energy to failure of the femur and can be performed minimally-invasively with less hospitalization costs and reduced recovery time [Beckmann et al., 2011; Fliri et al., 2012]. However, the side effects associated with femoroplasty may include thermal necrosis, toxicity of the cement, and embolism. [Efferiss et al., 1975] Injection of a large amount of cement, which has an exothermic curing process, may lead to osteonecrosis, i.e. death of bone tissue as a result of poor blood supply. Also suboptimal injection can result in bone weakening due to stress concentration, mainly at the cement-bone interface, and render the augmentation unsuccessful [Basafa and Armand, 2014]. Therefore it is desirable to use the minimum amount of cement possible to achieve the goals of augmentation.

It has been described the approach to computer-assisted planning of femoroplasty to optimize cement volume and placement (*Figure 8*) [Basafa and Armand, 2014]. In summary, it was showed that by introducing less than 10 ml of bone cement into the femur, it is possible to increase the yield load of the femur specimens by greater than 30%. [Basafa et al., 2015]

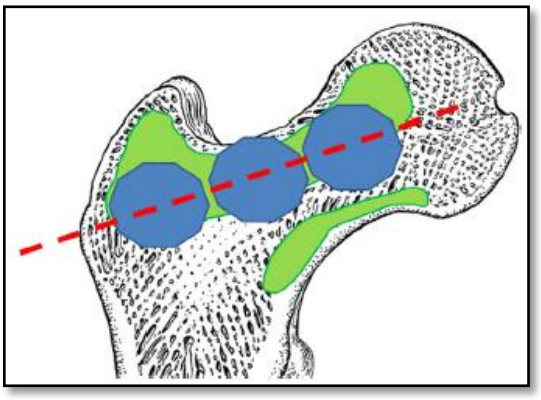

Figure 8: *Schematic of an augmentation suggested by simulations (green) and planned path and locations of injection (blue) [Basafa et al., 2015]*

Similar to vertebroplasty, femur augmentation can benefit from modelling and planning using computational techniques for biomechanical evaluation. (see Appendix I)

The planning procedure is summarized below:

- Create and analyze pre-planning FE model.
- Perform BESO (Bi-directional Evolutionary Structural Optimization) simulations and record the final cement pattern. The basic idea behind BESO is to gradually remove inefficient elements from a finite element domain and add elements to high load-bearing regions until convergence.
- Divide the femur into three regions, each containing several "test" points.
- Within each region, for each "test" point, simulate one injection. Select the point that overlaps most with the BESO pattern.
- Repeat the above step for all regions. For each step, use the updated CT of the previous region´s best point to re-create the porous model.
- Examine the points to determine the drill path(s). [Basafa and Armand, 2014]

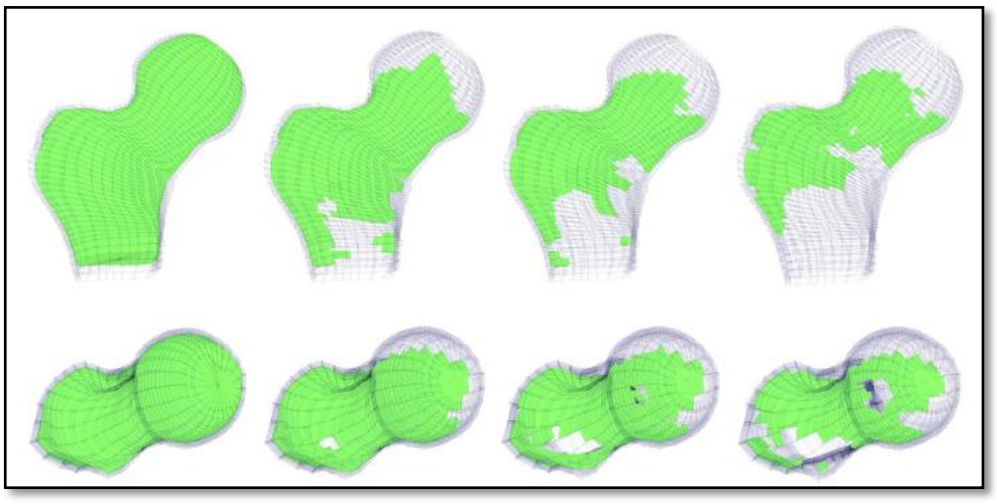

Figure 9: *From left to right: evolution of the cement placement (green elements) in a representative model [Basafa and Armand, 2014]*

A crucial step in the planning process is to determine the optimum volume and filling pattern of the cement so that the best outcome is achieved. [Basafa et al., 2013] A successful planning framework should hence include a module for predicting cement diffusion inside porous cancellous (spongy) bone.

In the more recent years, particle models have gained popularity for modeling fluid flows [Borau et al., 2014]. Among these models' advantages over grid-based methods are the inherent conservation of mass, no need for creating and maintaining a grid structure and fast computations of equations of motion. Because of their superior simulation speeds, particle models are of utmost interest in the graphics community and they have been used to model fluids and flow of colloids such as sand. [Basafa et al., 2013]

1.3 Objectives

Millions of fragility fractures occur directly because of osteoporosis, often at trabecular-dominant bone sites. Indeed, the trabecular bone plays an important role in load transmission and energy absorption in major joints such as the knee, hip, and spine. It is believed that, in addition to the bone volume fraction (the ratio of the volume of bone tissue to the overall bulk volume), the detailed microarchitecture, including trabecular orientation and connectivity, is important in governing the mechanical properties of trabecular bone [Wang et al., 2015]. The structure of open-cell rigid foams resembles that of human cancellous bone. The cell structure is over 95% open and the cell size is 1.5 to 2.5 mm. Furthermore, they are suitable for a variety of applications that require an open cell structure, such as dynamic testing or cement injection [Sawbones].

As regards cement injection, femoroplasty is a technique to prevent osteoporotic hip fractures by injecting acrylic bone cement, resulting in an increase of the mechanical properties of the trabecular bone.

Therefore, the main goal of this TFM is to carry out an in vitro and in silico characterization of open-cell structures for trabecular bone in order to plan and simulate the femoroplasty technique, so that we can know more about the associated osteoporotic failure mechanisms. Therefore, we will try to prevent osteoporotic fractures injecting bone cement in such open-cell structures. In order to achieve this main goal, secondary objectives are proposed:

- In vitro characterization of three types of open-cell structures
- In silico characterization of previous specimens
- Development of a discrete cement diffusion model
- Quantification of the mechanical properties of augmented open-cell structures

1.4 Structure

The TFM is structured as follows:

Chapter 1 is an introduction which describes the main concepts of the clinical scenario of trabecular bone and osteoporosis and its consequences on the bone tissue are detailed. Second, femoroplasty technique is reviewed and specific sequences in femur and, in particular, in trabecular bone are commented.

Chapter 2 describes the TFM methodology. It is divided in two main parts:

- **In vitro and in silico characterization of open-cell structures for trabecular bone,** in which specific details about experimental data acquisition, image processing, three-dimensional reconstructions and mechanical simulations based in finite element (FE) method are described.
- **Bone cement diffusion,** in which is proposed a new model based on the random-walk theory [Perez and Prendergast, 2007] in order to simulate augmentation process and to observe the improvement in mechanical properties in the open-cell structures for trabecular bone.

Chapter 3 shows the results of the application of the methodology proposed. The discussion is also presented.

Chapter 4 copes with the main conclusions of the TFM and also summarizes the possible lines of future work.

Three appendixes are included at the end in order to show relevant information that has not been included in the main document.

Chapter 2
Materials and methods

2.1 Introduction

In this chapter, we will try to explain the different steps to achieve our in vitro and in silico characterization of open-cell structures for trabecular bone. Therefore, we will begin this chapter showing the method that was used to perform the compression tests and obtain the mechanical properties of all open-cell structures. Then, Young´s Modulus and associated porosity will be also obtained using the FE method and comparing the results with the experimental ones. Finally, we will put forward a diffusion model, so that we can simulate the femoroplasty or cement injection technique. In addition, we will also quantify the mechanical properties of cemented open-cell structures.

2.2 In vitro and in silico characterization of open-cell structures for trabecular bone

2.2.1 Specimen preparation

We have three different specimens of open-cell structures (Sawbones, Malmö, Sweden) with the same size and different densities as we can see in Table 1 and *Figure 10*. From now on, we will refer to them as specimen #15 (Sawbones, product no. 1522-526-1, Malmö, Sweden), specimen #20 (Sawbones, product no. 1522-524, Malmö, Sweden), specimen #30 (Sawbones, product no. 1522-525, Malmö, Sweden).

The foams are produced by a polymerization reaction that takes place simultaneously with the generation of carbon dioxide by the reaction of water and isocyanate [Thompson et al., 2003]. The uniformity and consistency in their material properties make rigid polyurethane ideal for comparative testing [Shim et al., 2012].

Table 1: Specimen dimensions and densities

Specimen	Density (g/cc)	Base (mm)	Height (mm)	Thickness (mm)
#15	0.24	20	40	20
#20	0.32	20	40	20
#30	0.48	20	40	20

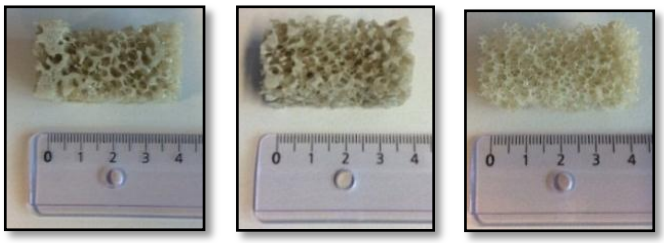

Figure 10: *On the left, specimen #30; in the middle, specimen #20; on the right, specimen #15*

2.2.2 Experimental data acquisition

The gold standard to determine bone competence is by assessing its mechanical properties in a functional mechanical test. It should be pointed out that all tested specimens were submitted to a quality control to ensure specimens´ homogeneity.

Uniaxial compression test (*Figure 11*) was used to obtain apparent Young´s moduli of all specimens.

Figure 11: *On the left, servo-hydraulic material testing machine; on the right, uniaxial compression test*

Fifty three cubic specimens (seventeen specimen #15, eighteen specimen #20 and eighteen specimen #30) were placed between steel plates at room temperature (approx. 23 °C) and loaded in the direction of their axis of symmetry. Compression experiments were conducted using a servo-hydraulic material testing machine (*Figure 11*) (Microtest, model EFH). The quasi static compression load was measured with a commercial load cell (10 kN) (*Figure 12*) applied at a constant velocity rate of 1 mm/min. [Keaveny et al., 1993]

Figure 12: *Commercial load cell (10 kN)*

The force displacement curves were measured for each test and the ultimate apparent stress (σ_u) and strain (ε_u) were calculated by:

$$\sigma_u = \frac{F_u}{A} \quad (2.1)$$

$$\varepsilon_u = \frac{\Delta L_u}{l_0} \quad (2.2)$$

where A, F_u, Δl_u and l_0 are respectively the apparent area of the specimen, the ultimate force at fracture (maximum of the force–displacement curve), the displacement at fracture (corresponding to the maximum of the force) and the initial height of the specimen. [Hambli, 2013]

2.2.3 Microcomputed tomography system and image processing

Firstly, among the fifty three specimens only eighteen (six of each type) were scanned with a microcomputed tomography system before compression tests (µCT50, General Electric), using a 50 µm nominal resolution to assess the trabecular bone architecture. In addition, it was obtained thresholds between 1000 for specimen #30 and 2000 for specimen #15. A Micro-computed Tomography (µCT) image captures the actual trabecular bone architecture from which three-dimensional connectivity, trabecular thickness, trabecular number and trabecular spacing can be obtained (*Figure 13*) [Hamed et al., 2012]. The scanned images were reconstructed using a semiautomatic reconstruction (MIMICS, Materialise NV, Leuven, Belgium). Thus, the finite element module was used to aid with segmentation of all specimens and to determine the volume fraction (*Figure 14*).

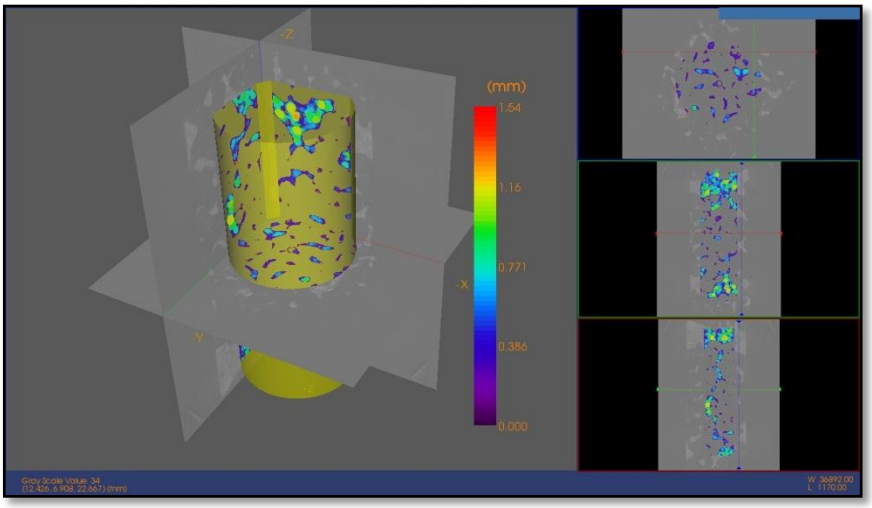

Figure 13: *Specimen #30 image capture*

All specimens were also digitally cut, to exclude bone fragments that might have resulted from the cutting process as well as to exclude unintentionally cut trabeculae.

Therefore, final specimen dimensions were 10 mm in base, 10 mm in height and 10 mm in thickness (10x10x10 mm). Furthermore, we could determine the volume fraction of the specimens in the module mentioned before. There was a wide range in bone volume fractions and trabecular architectures among the specimens.

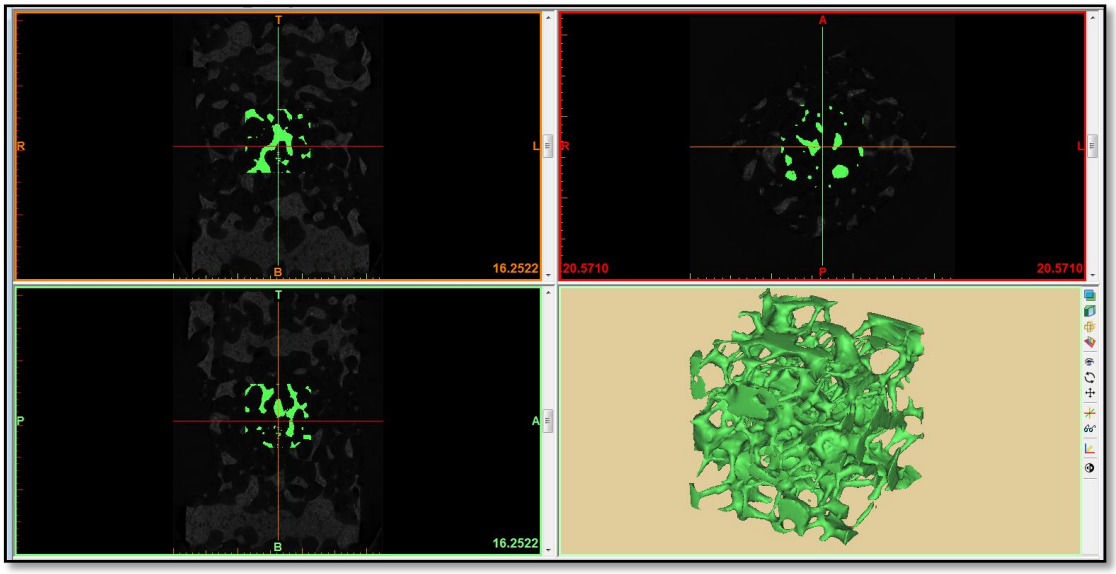

Figure 14: *Segmentation of CT data for each specimen using FE material assignment module in MIMCS (Materialise NV, Leuven, Belgium)*

2.2.4 Three dimensional reconstructions of the trabeculae

2.2.4.1 Generation of a linear and quadratic tetrahedral-based FE model

The two-dimensional surface elements are meshed into three-dimensional tetrahedral meshes for each specimen using 3-Matic tooling module (Materialise NV, Leuven, Belgium) (*Figure 15*) in which we could easily obtain linear and quadratic elements (*lin tet and quad tet*) to compare the influence of element types in elastic modulus. Finally, these meshes could be stored and exported to ABAQUS software (Dassault Systèmes Simulia Corp., Suresnes Frances) to perform the finite element analyses (FEA). (See Appendix I)

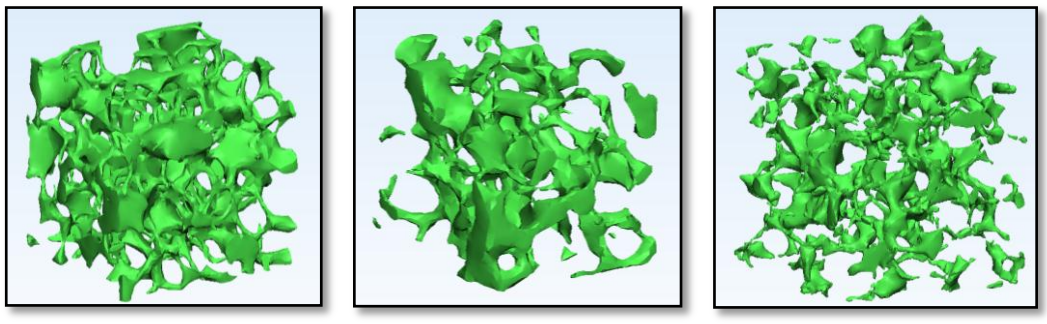

Figure 15: *Specimen #30 (on the right), specimen #20 (in the middle) and specimen #15 (on the right) in 3-Matic tooling module*

2.2.4.2 Generation of a voxel-based FE model

As we could observe in *Figure 16*, the thresholded μCT images of trabecular bone were converted to μFE models by transforming each voxel to 8-node brick element using the Voxel Create Mesh Module supplied by MIMICS (Materialise NV, Leuven, Belgium). It should be noted that *voxel* μFE models were based on the original μCT images of trabecular bone. It should be also pointed out that specimens were scanned along the height using a μCT scanner. The grayscale images were then down sampled to 120 μm voxel size and thresholded for further processing.

Figure 16: *Creation of voxel mesh for specimen #30 (on the right), specimen #20 (in the middle) and specimen #15 (on the right) using the Voxel Create Mesh Module*

2.2.5 Mechanical analysis using the FE method

The introduction of micromechanical finite element (μFE) models directly generated from micro-computed tomography (CT) reconstructions of trabecular bone have helped to determine its elastic properties [Van Rietbergen et al., 1995; Müller and Rüegsegger, 1995; Akhtar et al., 2006]. Now, it is possible to simulate a mechanical test over trabecular bone in great detail and with high precision [Van Lenthe et al., 2006].

After the mesh is constructed, the resulting FE models were imported into the commercial FE software package ABAQUS (Dassault Systèmes Simulia Corp., Suresnes Frances). In Appendix II it can be observed the mesh characterisitics for each specimen.

The bulk material is assumed to be linear elastic and isotropic with properties obtained in Table 2. Therefore, the elements of the FE meshes were assigned an arbitrary tissue modulus of 3200 MPa (E_{tissue}^{FE}). Poisson's ratio was defined as 0.3. Previous mechanical properties were provided by Sawbones (Sawbones, Malmö, Sweden).

Table 2: Mechanical properties of the bulk material

Specimen	Density (g/cc)	Modulus (MPa)	Strength (MPa)
Bulk material	1.56	3200	30

Boundary conditions for the FEM model idealize those of a uniaxial compression test [Wang et al., 2015]: a uniaxial displacement (uniform strain) is applied to the top surface of the cubic bone samples, the bottom surface is kept fixed [Van Lenthe et al., 2006] (*Figure 17*), while the sides are taken to be traction-free [Hamed et al., 2012]. An axial displacement was imposed which represented a strain of 2% (0.2 mm) [Wang et al., 2015]. In addition, contact between the upper and lower surfaces of the specimen and the plates were modeled using contact elements with a zero friction value to ensure that only compressive forces were transmitted. [Hambli, 2013]

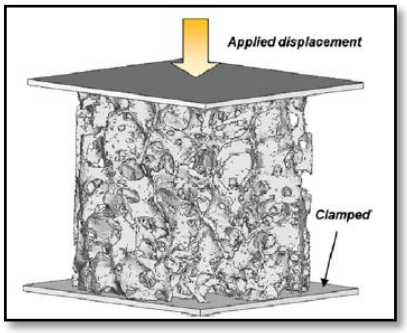

Figure 17: *FE model reproducing the compression [Hambli, 2013]*

Non-linear FE analyses were performed in ABAQUS v6.14 (Dassault Systèmes Simulia Corp., Suresnes Frances) and run in a computational cluster of 224 cores and 576 GB of RAM.

2.2.6 Processing of the results

After the FEA, the apparent modulus of each mesh type was calculated as:

$$E_{app}^{lin\ tet} = \frac{\sigma_{app}}{\varepsilon_{app}} = \frac{F/A}{\Delta L/L} \quad (2.3)$$

$$E_{app}^{quad\ tet} = \frac{\sigma_{app}}{\varepsilon_{app}} = \frac{F/A}{\Delta L/L} \quad (2.4)$$

$$E_{app}^{Voxel} = \frac{\sigma_{app}}{\varepsilon_{app}} = \frac{F/A}{\Delta L/L} \quad (2.5)$$

in which F is the force calculated from each FE simulation (N), A is the apparent specimen cross-section (mm^2), ΔL=0.2 mm and L is the specimen length *(L = 10 mm).*

On the other hand, we could estimate the associated porosities to all specimens using the next equations:

$$E_{app}^{lin\ tet} = E_{tissue}^{FE} \cdot (1 - P_{app}^{lin\ tet})^n \quad (2.6)$$

$$E_{app}^{quad\ tet} = E_{tissue}^{FE} \cdot (1 - P_{app}^{quad\ tet})^n \quad (2.7)$$

$$E_{app}^{Voxel} = E_{tissue}^{FE} \cdot (1 - P_{app}^{Voxel})^n \quad (2.8)$$

in which *n* was determined to be equal to 2 for an open-cell structure [Hamed et al., 2012]. Furthermore, we could also calculate and compare mentioned porosities with the porosity associated to specimen dimensions:

$$P_{sp} = \left(1 - \frac{V_{app}}{V}\right) \cdot 100 \quad (2.9)$$

where V_{app} is obtained from FE material assignment module in MIMCS (Materialise NV, Leuven, Belgium) and V is the specimen volume size without porous ($V \approx 1000$ mm^3), which is obtained after the 3D specimen reconstruction.

2.3 Bone cement diffusion

Augmentation of osteoporotic femur using PMMA bone cement to prevent or reduce the risk of fracture has been suggested to be an alternative preventive treatment (Section 1.2.2). Because of the possible complications, however, the procedure requires precise planning and execution. Effective planning relies, among others, on an accurate method for predicting the diffusion of the cement through the porous medium of osteoporotic cancellous bone. Our goal was to develop a discrete cement diffusion model based on the random-walk theory [Perez and Prendergast, 2007], that will simulate cement injection.

2.3.1 2D diffusion

An approach for modelling the bone cement diffusion based on the random-walk theory was developed [Perez and Prendergast, 2007]. It is a stochastic process. Initially, a cement particle was assumed (in two dimensions) to be surrounded by eight locations that a particle could occupy (*Figure 18*). Moved particles were not allowed to remain in the initial position. Therefore, this particle would be moved to another controlled location. We opted for an isotropic diffusion, that is, cement particles can occupy neighbouring positions with equal probability p (see *Figure 18*). Although *Figure 18* shows eight free positions around the initial cement particle, this will not, in general, be the case because some positions may be already occupied. Therefore the model incorporates "contact inhibition" by checking for vacant positions while cement particle moves and depending on the available states, the value of the probability p is computed in order to fulfil the condition $\sum_{i=1}^{n} p_i = 1$. If all the surrounded positions are free, the probability p given in *Figure 18* will be equal to 1/8. It should be pointed out that a cement particle will find more free

positions as diffusion increases. Basically, our model shows that diffusion increases as cement injection´s speed increases.

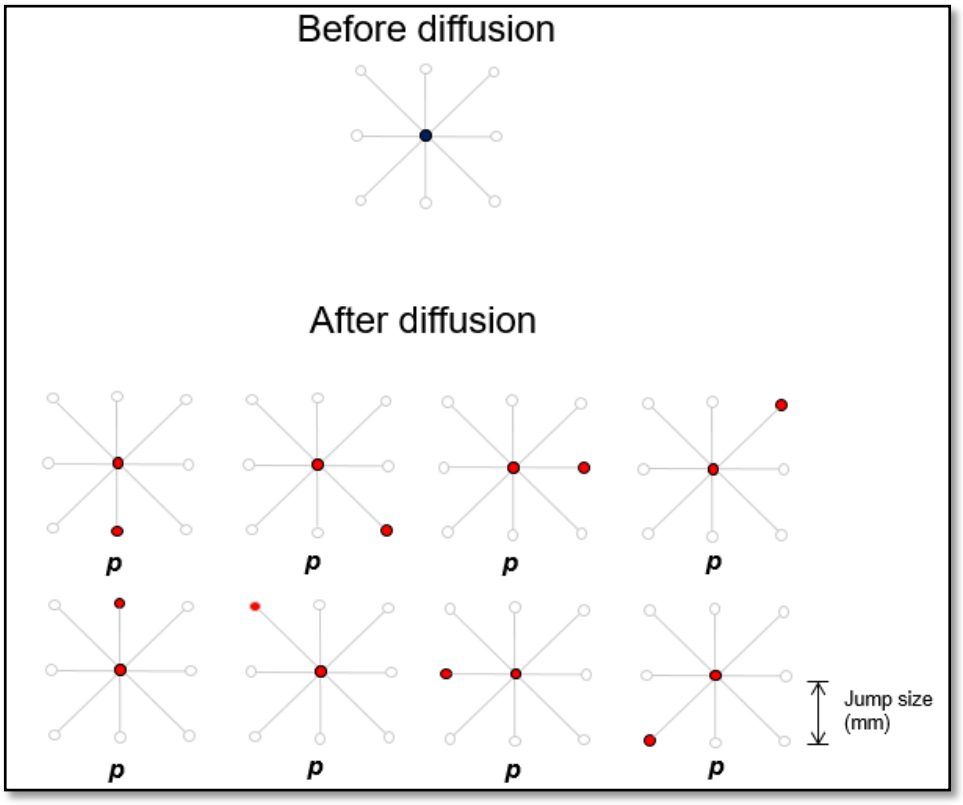

Figure 18: *Possible states that a bone cement particle can occupy after diffusion. The distance between the sites is only schematic; adjacent sites in the algorithm are considered to be exactly the jump size.*

In the stochastic model proposed, diffusion is controlled by some parameters:

- **Specimen size**
- **Number of injected cement particles**
- **Jump size**

At the end of the diffusion, the availability of the final position was checked. If it was not free, the surroundings positions to the final one were checked following the same approach. The determination of the probability values of the movement has been assumed to be phenomenological [Garijo et al., 2012].

In particular, to simulate cement diffusion in a 2D configuration, we used a matrix size of 100x100 in which we located bone positions (blue points) in random locations and then cement particles (red points) were injected following random trajectories, as it can be observed in *Figure 19*. In addition, as it was mentioned before, in any case these cement particles can´t fill bone positions. Therefore, it is checked in each iteration that the bone cement particles don´t occupy neither bone locations nor occupied cement locations.

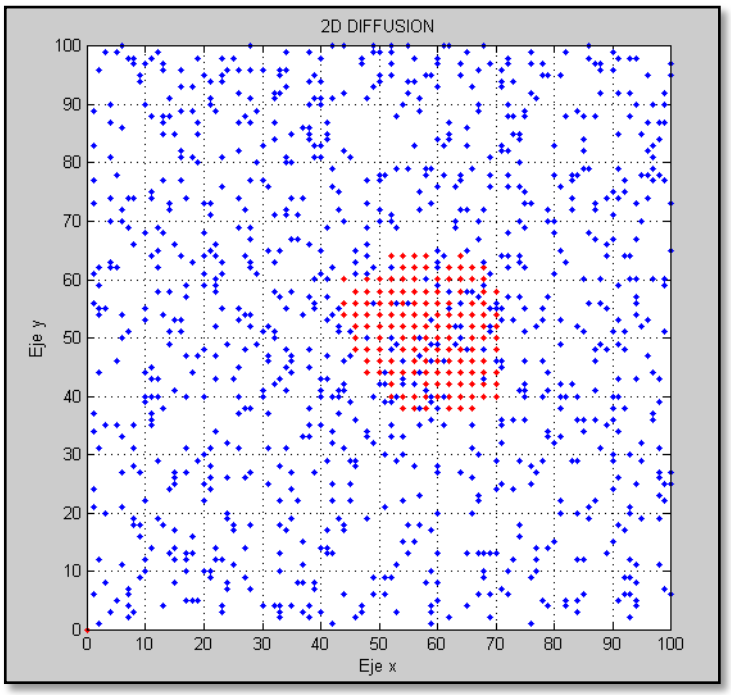

Figure 19: *Simulation of 2D diffusion*

2.3.2 3D diffusion

As it was obtained in a 2D configuration, 3D cement diffusion was also obtained based on the random-walk theory explained before, but extrapolated to 3D space (*Figure 20*) (Section 2.7.1) [Perez and Prendergast, 2007]. In this case, a cement particle was presumed (in three dimensions) to be surrounded initially by 24 locations (8 locations in each plane) that a particle could occupy. Therefore, if all surrounded positions are free, the probability *p* will be equal to 1/24.

In this model proposed, diffusion is controlled by some parameters, as it was mentioned in 2D diffusion

- **Specimen size:** it will be the specimen size of the voxel-based FE models in each plane.
- **Number of injected cement particles:** this number will depend on the specimen size and will be obtained through the following expression:

$$N_{injected\ particles} = \frac{T \cdot V}{V_{Voxel}} \qquad (2.10)$$

where V is the specimen volume size without porous ($V \approx 1000$ mm^3), T is the amount that it is supposed that it should be injected (5% or 20%) [Basafa et al.,

2015] in the specimen and V_{voxel} is the voxel volume size. Each voxel, based on CT scans acquired, had the dimensions 0.12x0.12x0.12 mm^3.

- **Jump size:** distance that a particle covers in each jump.

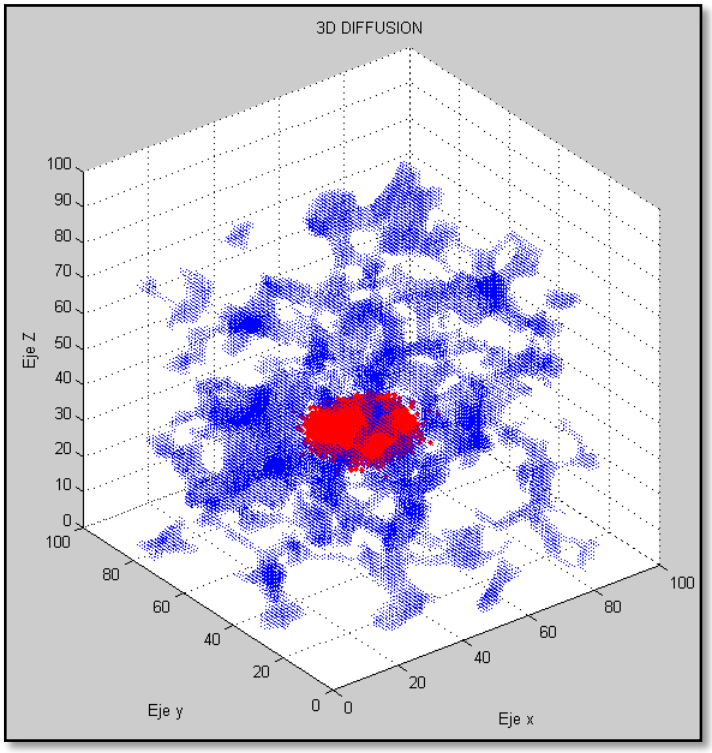

Figure 20: *Simulation of 3D diffusion in specimen #15*

2.3.3 Mechanical simulation of compressive conditions

To further test the model, we performed three injection simulations (one at each specimen type) in a setting similar to osteoporotic bone augmentations, inspired by the experiments of Loeffel et al. and Basafa et al. (2013). The goal was to perform precisely controlled injections comparing the results between the mechanical properties obtained before and after cement augmentation.

Boundary conditions were the same which were showed in Section 2.2.5. It was assumed that the compressive Young's modulus of pure PMMA is 2.0±0.1 GPa [Kim et al., 2004]. Therefore, the bone cement elements of the voxel-based FE meshes were assigned an arbitrary modulus ($E^{FE}_{bone\ cement}$) of 2000 MPa. Bone cement Poisson's ratio was defined as 0.3.

2.3.4 Processing of the results

After the FEA, the apparent modulus of cemented specimens was calculated as:

$$E_{app}^{Voxel\ (bone\ cement)} = \frac{\sigma_{app}^{Voxel\ (bone\ cement)}}{\varepsilon_{app}^{Voxel\ (bone\ cement)}} = \frac{F/A}{\Delta L/L} \quad (2.11)$$

in which F is the force calculated from each FE simulation (N), A is the apparent specimen cross-section (mm^2), ΔL=0.2 mm and L is the specimen length *(L = 10 mm).*

Chapter 3

Results and discussion

3.1 Experimental results

At the beginning, we have three different open-cell structures supplied by Sawbones (Sawbones, Malmö, Sweden) with the same size, but different volume fractions (Table 3). In addition, Sawbones (Sawbones, Malmö, Sweden) provided us with all the information related to open-cell structures. Therefore, the experimental and computational validation of them is one of our goals in this TFM.

Table 3: Mechanical properties of open-cell structures (Sawbones, Malmö, Sweden)

Specimen	Volume fraction	E Sawbones (MPa)
#15	0.15	53
#20	0.21	105
#30	0.31	270

As regards the experimental results of compressive tests (Table 4), the experimental data clearly show an increase in Young´s Modulus with bone volume fraction (*Figure 21*). Furthermore, our experimental results for Young´s Modulus are close to the values provided by Sawbones (Sawbones, Malmö, Sweden) depending on the volume fraction (Table 3). Results obtained for specimen #15 and #20 are high accurate. However, specimen #30 has a lower Young´s Modulus in our experiments if we compare them with the data provided by Sawbones (Sawbones, Malmö, Sweden). A reason for the poor results of our experimental data in specimen #30 may be systematic errors in the platen compression test of trabecular bone, which occur owing to end artefacts and specimens defects associated to manufacturing process. Such errors lead to an underestimation of compressive Young´s Modulus of trabecular bone [Hamed et al., 2012] in the specimen #30.

Table 4: Experimental results of Young´s Modulus from compressive tests (to know more information about the experimental results, we recommend seeing Appendix III)

Specimen	Volume fraction	E Sawbones (MPa)	E experimental (MPa)
#15	0.15	53	62.74 ± 17.08
#20	0.21	105	111.35 ± 34.98
#30	0.31	270	187.47 ± 87.12

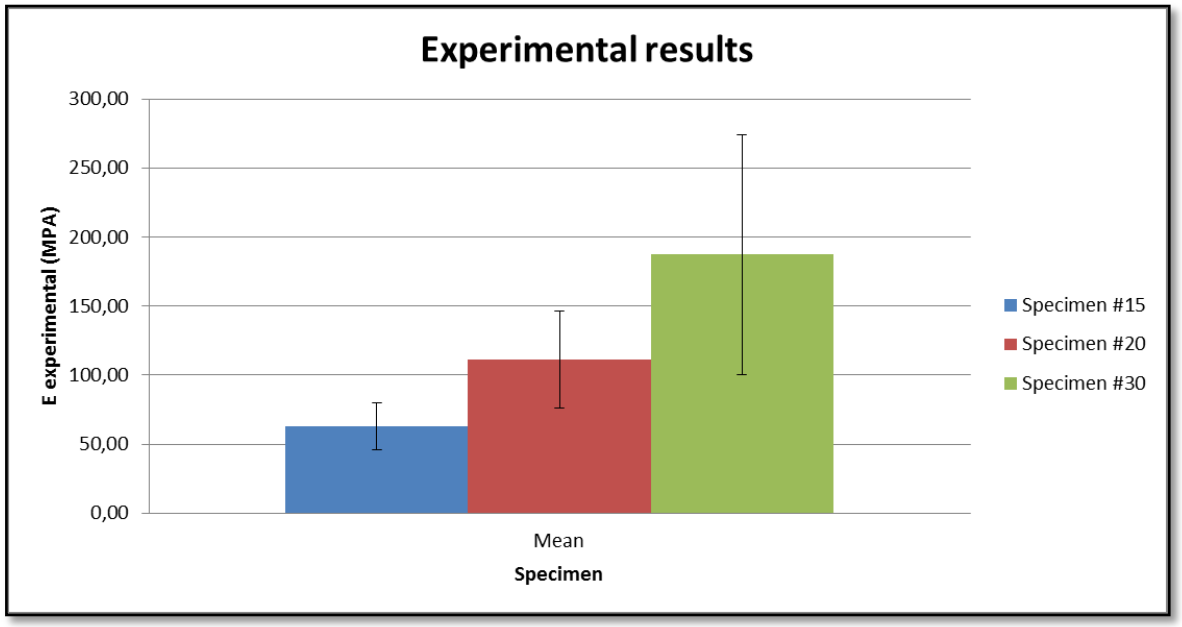

Figure 21 : *Experimental results from compressive tests*

As it was mentioned in section 2.2.2, all tested specimens were submitted to a quality control to ensure specimens´ homogeneity. Because of the complex geometry of specimens, machining bone samples may cause significant surface defects [Hamed et al., 2012] that may result in a reduction of the mechanical properties of the specimen, that is, a reduction in the Young´s Modulus.

However, it can be observed that in some cases Young´s Modulus increases its value significantly, because the progressive contact of broken trabeculae during the compression test leads to increase the load carrying capacity. [Hambli, 2013] (See Appendix III)

Direct mechanical testing is a straight-forward procedure, but has its limitations as it is a destructive test. Therefore, this method is not applicable in vivo. And although it can be used to test specimens in vitro, a specimen can only be tested once, thereby limiting the assessment of direction-dependent characteristics. Furthermore, these tests are prone to errors, related to boundary artifacts and to the often small size of the specimens, hampering high precision, especially for bones of small animals. [Hamed et al., 2012] It is clear that

specimen shape greatly influences mechanical properties of trabecular bone [Pace et al., 2014] as it has been observed in our experiments.

3.2 In silico results

As it was mentioned before (Section 2.2.3), only eighteen specimens (six of each volume fraction) were scanned with a microcomputed tomography system before compression tests. Then, FE analyses were performed in those specimens. It should be pointed out that FE reconstructions were carried out, as it was detailed in Section 2.2.4. Therefore, the mechanical properties of each specimen were assessed, that is, the predicted apparent Young´s Modulus and the estimated porosities were represented in Table 5 and Table 6, respectively.

Table 5: Young´s Modulus (MEAN ± SD) obtained using finite element analysis for all specimens

Specimen	Dimensions (mm)	$E_{app}^{lin\ tet}$(MPa)	$E_{app}^{quad\ tet}$(MPa)	E_{app}^{Voxel}(MPa)
#15	10x10x10	89.93 ± 62.33	67.15 ± 48.54	85.89 ± 54.69
#20	10x10x10	118.67 ± 62.96	121.38 ± 73.91	121.16 ± 67.01
#30	10x10x10	257.57 ± 110.93	228.58 ± 106.68	178.05 ± 96.61

Table 6: Estimated porosities (MEAN ± SD) obtained using finite element analysis for all specimens

Specimen	Dimensions (mm)	P_{sp} (%)	$P_{app}^{lin\ tet}$(%)	$P_{app}^{quad\ tet}$(%)	P_{app}^{Voxel}(%)
#15	10x10x10	83.21 ± 9.76	84.15 ± 5.97	86.38 ± 5.42	84.55 ± 5.98
#20	10x10x10	80.31 ± 7.25	79.15 ± 5.82	79.75 ± 6.33	79.15 ± 6.07
#30	10x10x10	76.59 ± 10.64	72.30 ± 6.73	74.02 ± 6.88	77.38 ± 7.32

As regards apparent Young´s Modulus (Table 5), we could observe that depending on the mesh type used to perform the finite element analysis, different values of apparent Young´s Modulus could be obtained. For instance, it could be assessed that quadratic tetrahedral elements were more suitable to represent the real mechanical properties of those specimens that possessed lower volume fractions (*Figure 22*), but it also existed an overestimation of apparent Young´s Modulus. The use of quadratic tetrahedral elements resulted in a reduction of the inherent stiffness of linear tetrahedral elements. On the other hand, linear tetrahedral elements were capable of representing in an acceptable way the real mechanical properties of specimens with higher volume fractions (*Figure 24*), but it also exists an underestimation of apparent Young´s Modulus. In the same way, we observed that regardless of the mesh type used to perform the finite element analyses, volume fractions near 0.20 (*Figure 23*) showed similar results of Young´s Modulus and estimated porosity to real cases. Despite these results, we could observe that standard deviations seemed to increase their values as volume fraction got higher.

In fact, in the present study we found that the variance in volume fraction in a single specimen can be relatively large [Stauber et al., 2014]. It is a fact that FE predictions of apparent modulus were already reported to be strongly affected by the threshold used for segmentation of CT data to create the FE mesh [Hara et al., 2002], and are extremely sensitive to errors due to the power relationship between volume fraction and mechanical properties. Another assumption is related to the constitutive behavior of trabecular bone tissue. In this case, the anisotropic nature of trabecular bone tissue has been simplified. This can lead to errors due to modelling hypotheses and experimental errors in the compression test procedures [Keaveny et al., 1997], and in some cases (*Figure 24*), have resulted in surprisingly low values of tissue modulus [Hou et al., 1998; Ladd et al., 1998]. [Chevalier et al., 2007]

As regards estimated porosities (Table 6), it exists large correlations between estimated and real porosities whatever the mesh type is used (*Figure 22*, *Figure 23*, *Figure 24*). In addition, it should be pointed out that mean porosities and standard deviations seemed to increase as volume fraction got higher (specimen #30). On the other hand, porosity results showed that linear tetrahedral elements were more suitable to represent the real porosity of specimen #30.

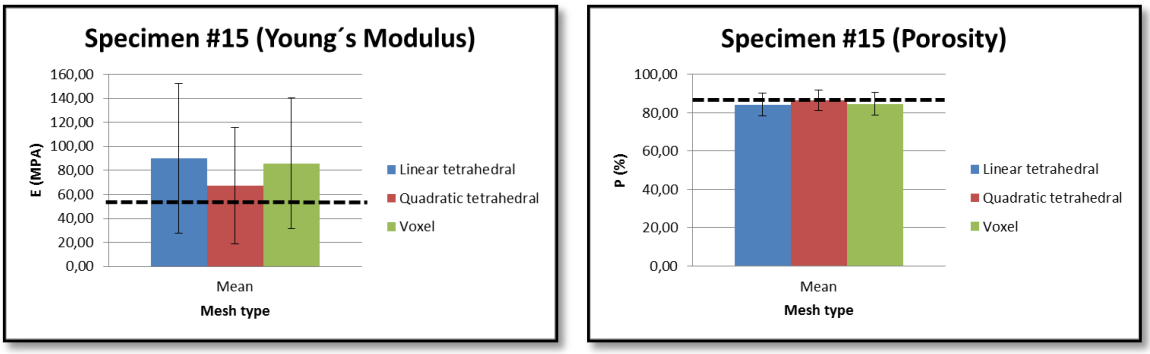

Figure 22: *Graphic representation of apparent Young´s Modulus (on the left) and estimated porosity (on the right) of specimen #15 for the different mesh types considered. Dashed line represents Sawbones (Sawbones, Malmö, Sweden) specifications*

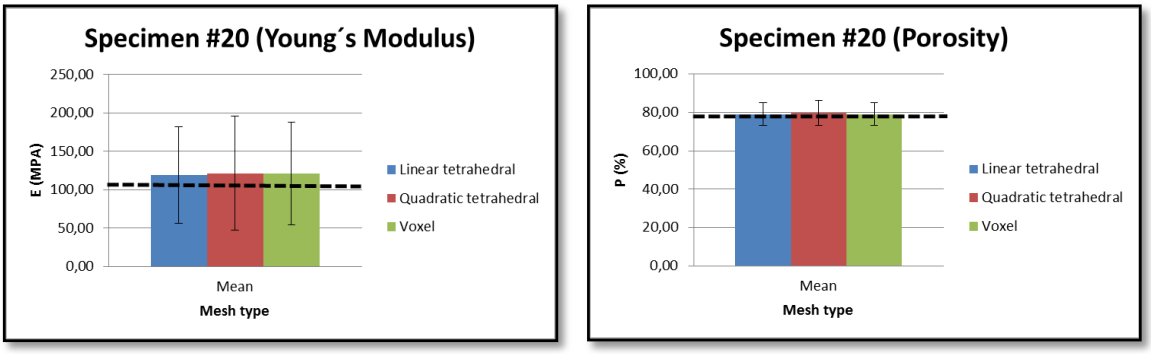

Figure 23: *Graphic representation of apparent Young´s Modulus (on the left) and estimated porosity (on the right) of specimen #20 for the different mesh types considered. Dashed line represents Sawbones (Sawbones, Malmö, Sweden) specifications*

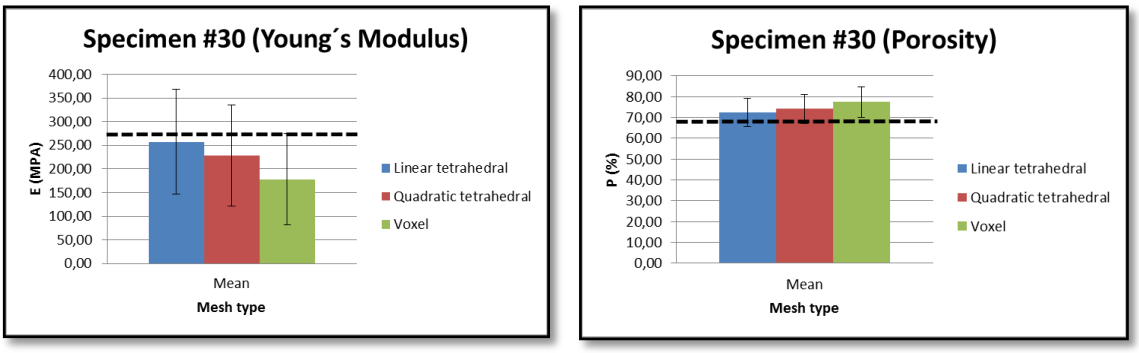

Figure 24: *Graphic representation of apparent Young´s Modulus (on the left) and estimated porosity (on the right) of specimen #30 for the different mesh types considered. Dashed line represents Sawbones (Sawbones, Malmö, Sweden) specifications*

Furthermore, it was believed that it was necessary to show a comparison between experimental and computational Young´s Modulus (Table 7) and between associated porosity to specimen dimensions and estimated porosity of each specimen (Table 8). It should be pointed out that it has even been obtained correlations between experimental and computational Young´s Modulus of $R^2 = 0.8027$ close to literature ($R^2 = 0.8541$) [Hambli, 2013] (*Figure 26*). However, as it was mentioned before, we have observed some differences depending on the mesh type used to perform the finite element analyses. Specimens #15 (*Figure 25*) showed better results when quadratic tetrahedral elements were used. On the other hand, specimen #20 (*Figure 26*) had higher correlations between experimental and computational data when the analyses were run with linear tetrahedral elements. Finally, voxel elements showed in a better way the mechanical properties of specimen #30 (*Figure 27*). However, it could easily observe that both correlations between experimental and computational Young´s Modulus and correlation between associated porosity to specimen dimensions and estimated porosity, showed poor results, but similar to those obtained in the literature. For instance, Ulrich et al., 1998 obtained that the moduli was underestimated by less than 41% with a standard deviation of 19%.

Table 7: Correlation between experimental and computational Young´s Modulus depending on the mesh type was used to perform the finite element analyses

Specimen	$R^{2(\text{lin tet})}_{app}$	$R^{2(\text{quad tet})}_{app}$	$R^{2(\text{Voxel})}_{app}$
#15	0.3261	0.4025	0.1960
#20	0.8027	0.4895	0.4090
#30	0.2554	0.5185	0.3793

Table 8: Correlation between associated porosity to specimen dimensions and estimated porosity depending on the mesh type was used to perform the finite element analyses

Specimen	$R^{2(\text{lin tet})}_{app}$	$R^{2(\text{quad tet})}_{app}$	$R^{2(\text{Voxel})}_{app}$
#15	0.3567	0.4564	0.2283
#20	0.6331	0.5509	0.5150
#30	0.0341	0.1129	0.1627

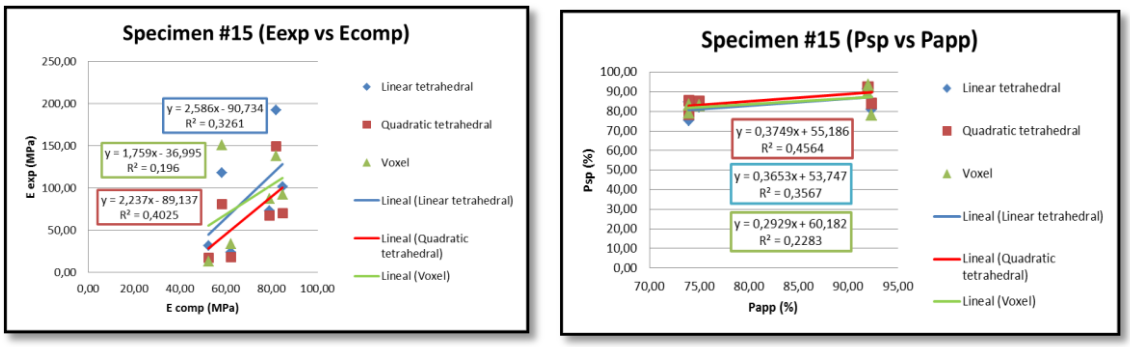

Figure 25: *Graphic comparison between experimental and computational Young´s Modulus (on the left) and between associated porosity to specimen dimensions and estimated porosity (on the right) of specimen #15*

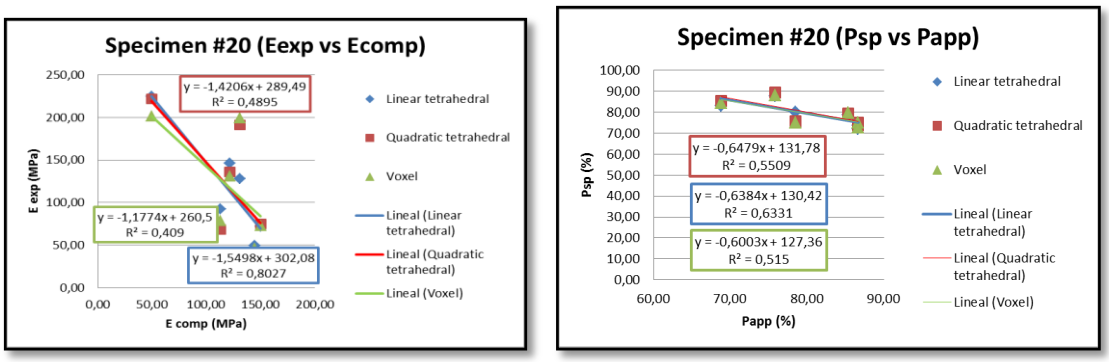

Figure 26: *Graphic comparison between experimental and computational Young´s Modulus (on the left) and between associated porosity to specimen dimensions and estimated porosity (on the right) of specimen #20*

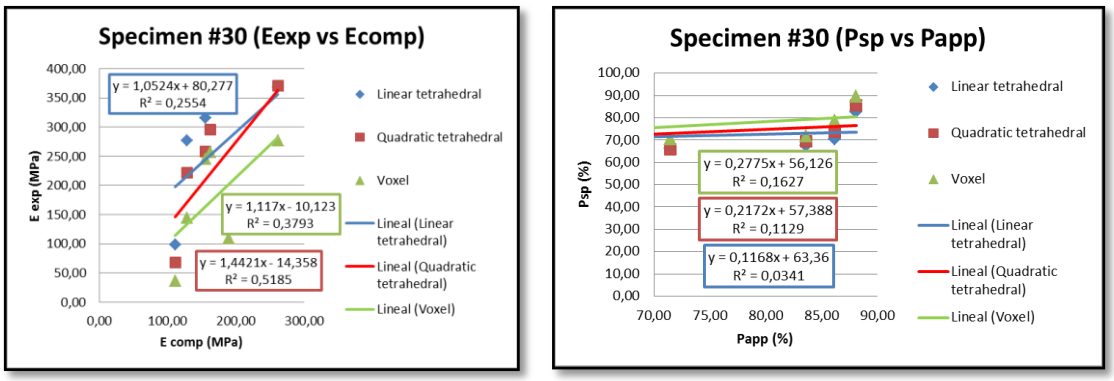

Figure 27: *Graphic comparison between experimental and computational Young´s Modulus (on the left) and between associated porosity to specimen dimensions and estimated porosity (on the right) of specimen #30*

3.3 Cement diffusion results

As it was mentioned in Section 2.3, augmentation of osteoporotic femur has been suggested to be an alternative preventive treatment. The development of a discrete cement diffusion model based on the random-walk theory [Perez and Prendergast, 2007] will allow us to to perform precisely controlled injections comparing the results between the mechanical properties obtained before and after cement augmentation.

In order to assess the improvement in the mechanical properties of augmented specimens, we compared $E_{app}^{Voxel\,(bone\ cement)}$ and E_{app}^{Voxel} obtained before (Table 5), so that we could easily observe that specimens with lower volume fractions showed a considerable increase in the mechanical properties as cement injection got higher (Table 9) (*Figure 29*) [Rubin et al., 2002]. On the other hand, in *Figure 28* it can be observed that strains are lower in specimens #15, as cement injection increase. In contrast, in specimen #30, the increase in cement injection hardly varied neither Young´s Modulus nor strains.

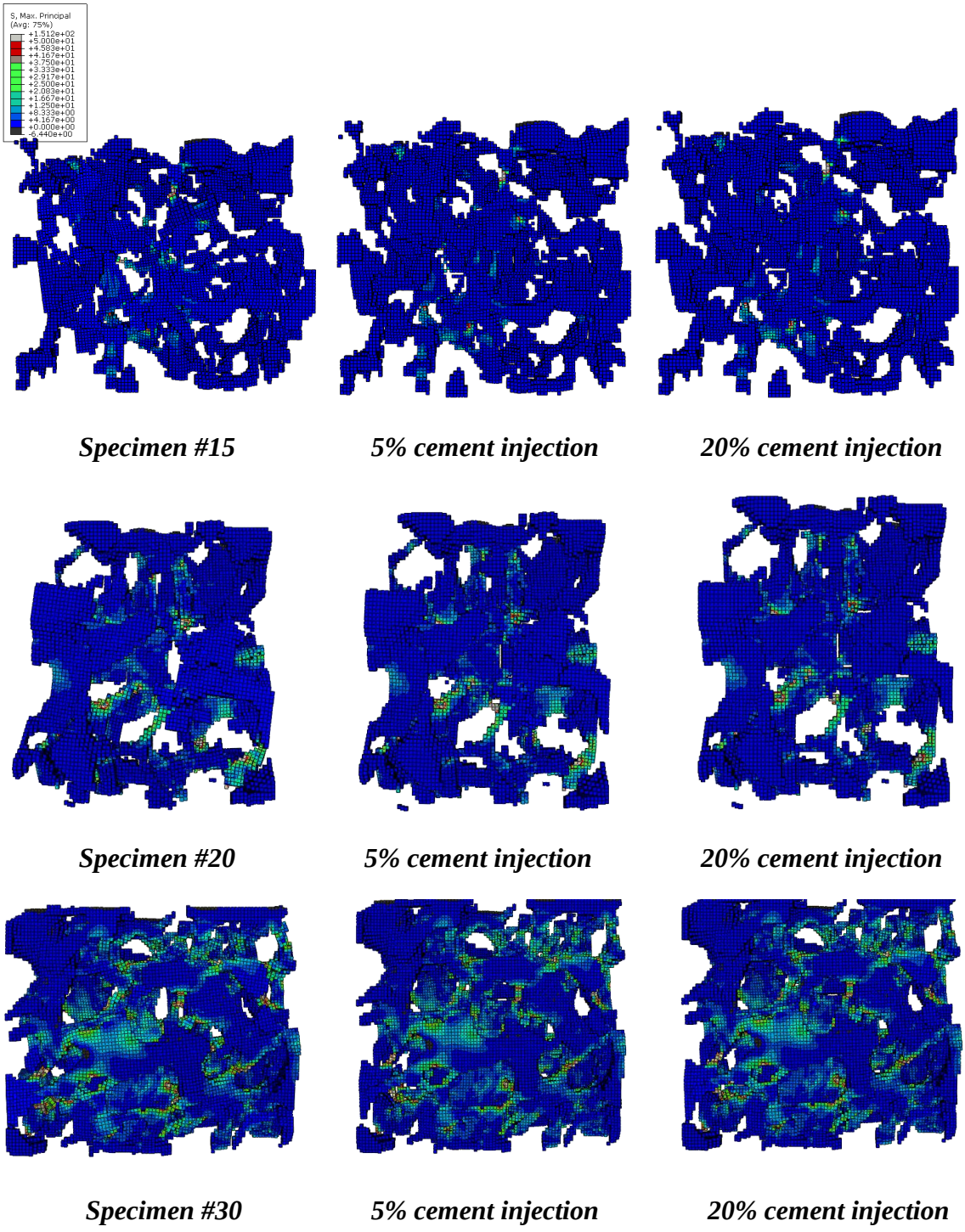

Figure 28: *Principal Maximum Stress Distribution in specimen #15, specimen #20 and specimen #30*

Table 9: Improvement of the mechanical properties of augmented specimens (%)

Specimen	5% injection (%)	20% injection (%)
#15	0.80	13.33
#20	3.81	5.43
#30	1.02	1.58

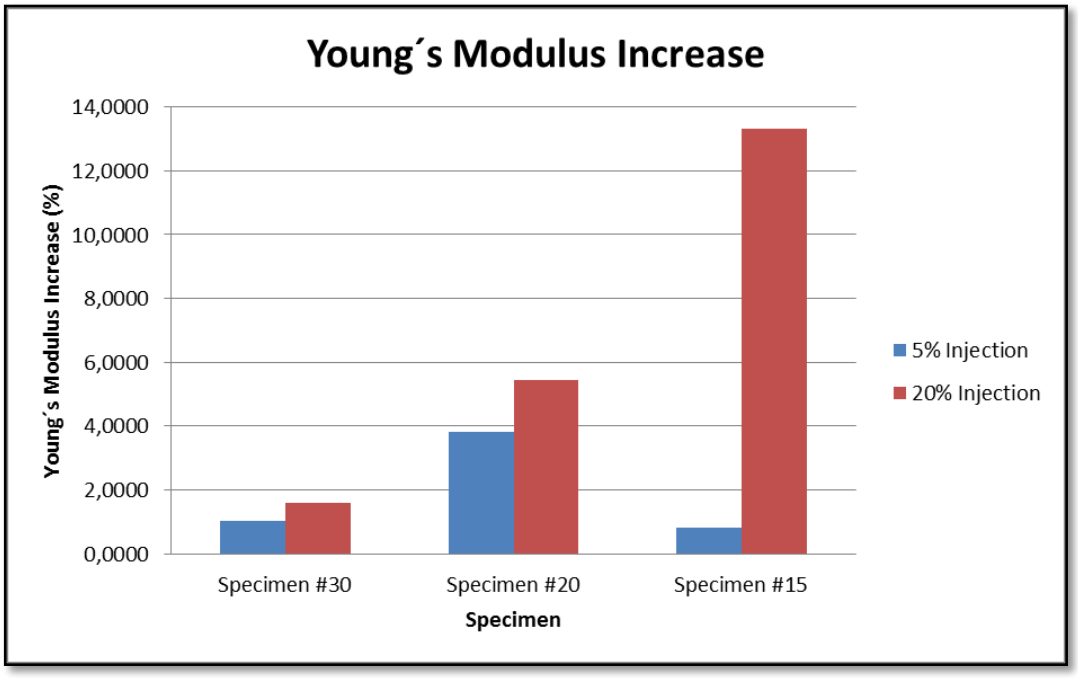

Figure 29: *Graphic representation of the improvement of the mechanical properties of augmented specimens*

Chapter 4

Conclusions and future work

4.1 In vitro and in silico characterization of open-cell structures for trabecular bone

In this TFM we obtained experimental and computational results throughout compression tests and Finite Element Analyses (FEA), respectively. Therefore, the model was validated with experimental results performed on the fifty-three specimens and with computational results performed on eighteen specimens. A major strength of this study was the use of specimens with large variations in microarchitecture and bone volume fraction for experimental validation (Table 1). Furthermore, we proposed a cement diffusion model based on the random-walk theory [Perez and Prendergast, 2007], validating its efficacy through simulations inside porous cancellous bone.

Firstly, to assess specimens, experimental tests have been proposed. Basically, compression tests in a servo-hydraulic material testing machine have been used to assess apparent Young´s Modulus.

As regards the experimental results of compressive tests (Table 4), the experimental data clearly show an increase in Young´s Modulus with bone volume fraction (*Figure 21*). Furthermore, our experimental results for Young´s Modulus are on the high side and on the lower side of the values provided by Sawbones (Sawbones, Malmö, Sweden) depending on the volume fraction. Hamed et al., (2012) showed that machining bone samples may cause significant surface defects that may result in a reduction of the mechanical properties of the specimen, that is, a reduction in the Young´s Modulus (specimen #30). In fact, our initial specimens (20 x 20 x 40 mm) were cut from a higher specimen with a volume size of 40 x 40 x 40 mm. Additionally, Dendorfer et al., (2008) showed that the accumulation of trabecular tissue damage and fracture affects the induced force–displacement curve of the whole specimen. Furthermore, Hambli (2013) observed that in some cases Young´s Modulus increases its value significantly, because the progressive contact of trabeculae generates the compaction of the specimen microstructure (specimen #15). Despite these limitations, experimental results are considered to be in agreement with the mechanical properties provided by Sawbones (Sawbones, Malmö, Sweden).

Secondly, micromechanical finite-element models have been used and continue being an important simulation tool. They help to interpret the results of mechanical tests and could reduce in vitro testing. Although, we should take into account the numerical errors and uncertainties that occur with these methods [Ladd and Kinney, 1998; Hamed et al., 2012].

Challenges and issues in creating FEM model might give rise to some errors in estimating Young´s modulus of trabecular bone or in this work, of open-cell structure. The first challenge is how to set a threshold value for μCT images to accurately capture bone architecture and porosity. Thresholding determines whether a partially filled voxel is considered as bone or void. This might cause some errors in calculating a bone volume fraction which could be carried over into a finite-element model. Finally, the resolution of our μCT image was selected to be 50 μm. Finer resolution would certainly capture better the trabecular bone architecture and lead to more accurate FEM predictions. Then, we compared our computational results (Table 5, Table 6) with the experimental data (Table 4) obtained using the same specimen.

Our results indicate differences among the element type used for the FEA (linear tetrahedral vs quadratic tetrahedral vs voxel mesh). For instance, it could be assessed that quadratic tetrahedral elements were more suitable to represent the real mechanical properties of those specimens that possessed lower volume fractions (high porous structures). On the other hand, linear tetrahedral elements were capable of representing in an acceptable way the real mechanical properties of specimens with higher volume fractions (low porous structures). In the same way, we observed that regardless of the mesh type was used to perform the finite element analyses, volume fractions near 0.20 (*Figure 23*) showed similar results of Young´s Modulus and estimated porosity to real cases. Despite these results, we could observe that standard deviations seemed to increase its values as volume fraction got higher. Therefore, we believe that linear tetrahedral meshes are better to simulate specimen which have volume fractions higher than 0.20. In contrast, quadratic tetrahedral meshes are more suitable in those cases which volume fractions are lower than 0.20.

As regards estimated porosities (Table 6), it exists large correlations between estimated and real porosities whatever the mesh type is used (*Figure 25*, *Figure 26*, *Figure 27*). In addition, it should be pointed out that mean porosities and standard deviations seemed to increase as volume fraction got higher (specimen #30). On the other hand, porosity results showed that linear tetrahedral elements were more suitable to represent the real porosity of specimen #30.

On the other hand, if we compare experimental and computational results in each specimen, it should be pointed out that we have also observed some differences depending on the mesh type used to perform the finite element analyses. Specimen #15 (*Figure 25*) showed better results when quadratic tetrahedral elements were used. On the other hand, specimen #20 (*Figure 26*) had higher correlations when the analyses were run with linear

tetrahedral elements. Finally, voxel elements showed in a better way the mechanical properties of specimen #30 (*Figure 27*). However, it existed poor results, but similar to those obtained in the literature. [Ulrich et al., 1998]

As regards specimen #30, the accuracy of FE voxel models seems more crucially affected by geometrical factors (region of analysis and segmentation) than material properties at low trabecular density, but at higher volume fractions geometrical and material properties appear equally important. Consequently, in performing analyses with such FE models, one should not only be careful in determining material properties and generating the trabecular geometry from the CT images, but more importantly should include the full geometry of the region of interest in order to minimize associated errors. [Chevalier et al., 2007]

If we observe the advantages and disadvantages of each mesh type, we can conclude that linear tetrahedral meshes are better to simulate specimen which have volume fractions higher than 0.20, because these elements allowed results more closely to theoretical ones [Ramos and Simoes, 2006]. In contrast, quadratic tetrahedral meshes are more suitable in those cases which volume fractions are lower than 0.20.

4.2 Bone cement diffusion

As regards bone cement diffusion, we have developed a discrete diffusion cement model based on the random-walk theory [Perez and Prendergast, 2007], that allowed us to simulate the cement diffusion in osteoporotic bones with a high risk of fracture. In addition, we carried out some FEA simulations in augmented specimens. We could observe that specimens with lower volume fractions even improved their mechanical properties in a 13.33%. For instance, similar results were obtained by Rubin et al. (2002), who achieved an improvement of 12.1 %. In contrast, specimens with higher volume fractions showed a lower increase in Young´s Modulus (Table 9).

4.3 Future work

In a future work, MIMICS (Materialise NV, Leuven, Belgium) will be used to segment and export an important amount of specimen meshes that let us understand more about the trabecular bone failure. In particular, segmentation of trabecular bone and bone cement will help us to simulate the augmentation technique in femoroplasty.

Furthermore, we will carry out mechanical tests of cemented specimens, that is, we will inject bone cement in some open-cell structures with different porosity, which will be compressed to failure in one of three orthogonal directions. This fact will allow us to validate the 3D discrete cement diffusion model.

Later we will also be able to do a multiscale model capable of predicting the fracture risk at pre-and post-femoral cementing phases. It will be developed and validated against in vivo assays.

Finally, using a previously developed patient-specific parametric model of the human proximal femur, a multiscale methodology will be developed to estimate the most appropriate preventive treatment to help reduce the risk of fracture (*Figure 30*).

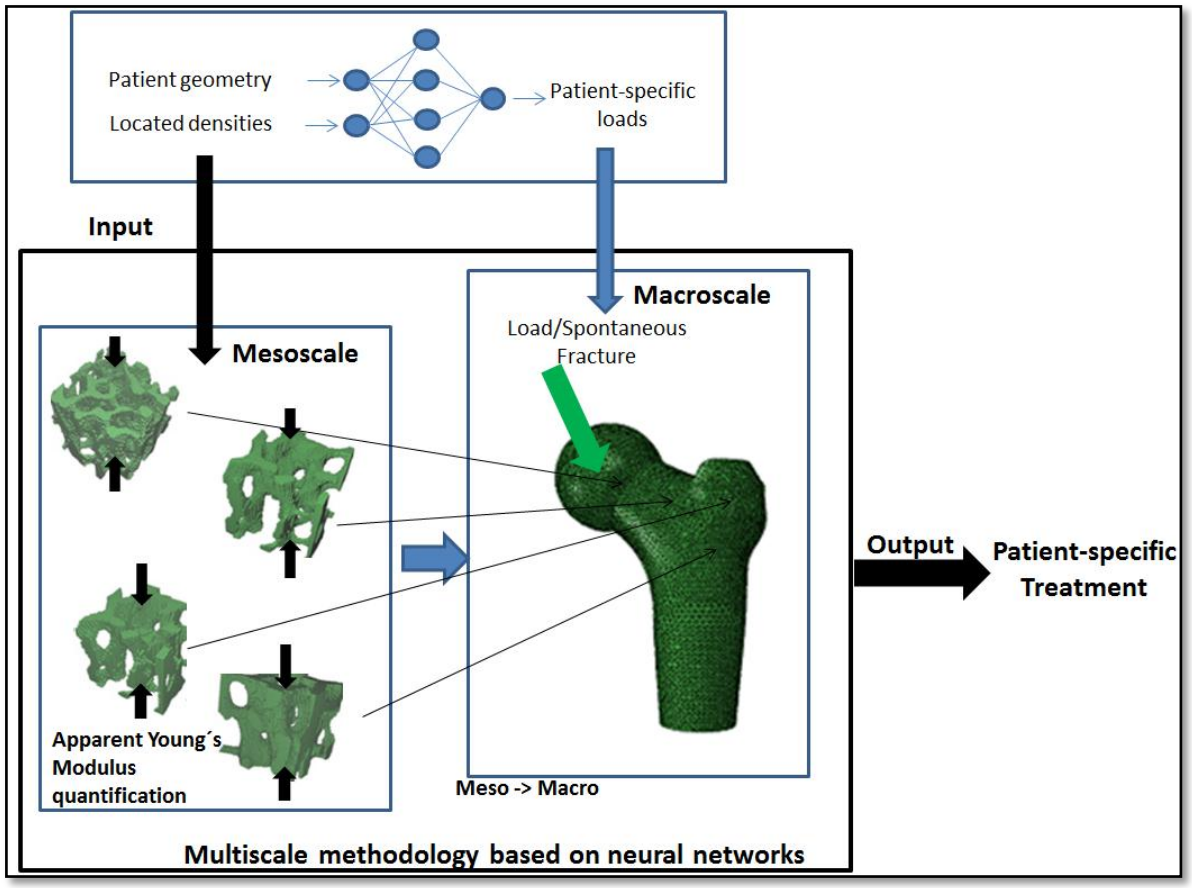

Figure 30: *Multiscale model capable of predicting the fracture risk at pre-and post-femoral cementing phases*

References

[1] A TextBook of Histology (12th Edition). Fawcett DW (ed). New York, NY: Chapmann & Hall, 1994.

[2] Akhtar, R., Eichhorn, J., Mummery, P.M. (2006) Microstructure-based finite element modelling and characterization of bovine trabecular bone. Journal of Bionic Engineering, 3, 3-9.

[3] Alberich Bayarri, Ángel (2010). In vivo morphometric and mechanical characterization of trabecular bone from high resolution magnetic resonance imaging.

[4] Available at http://www.sawbones.com/Catalog/Biomechanical/Biomechanical%20Test%20Materials/1522-524].

[5] Baron R. Anatomy and ultrastructure of bone. In: Favus MJ (ed) Primer on the metabolic bone diseases and disorders of mineral metabolism. New York, NY: Raven, 2003.

[6] Basafa, E., & Armand, M. (2014). Subject-specific planning of femoroplasty: A combined evolutionary optimization and particle diffusion model approach.Journal of biomechanics, 47(10), 2237-2243.

[7] Basafa, E., Armiger, R. S., Kutzer, M. D., Belkoff, S. M., Mears, S. C., & Armand, M. (2013). Patient-specific finite element modeling for femoral bone augmentation. Medical engineering & physics, 35(6), 860-865.

[8] Basafa, E., Murphy, R. J., Kutzer, M. D., Otake, Y., & Armand, M. (2013). A particle model for prediction of cement infiltration of cancellous bone in osteoporotic bone augmentation. PloS one, 8(6), e67958.

[9] Basafa, E., Murphy, R. J., Otake, Y., Kutzer, M. D., Belkoff, S. M., Mears, S. C., & Armand, M. (2015). Subject-specific planning of femoroplasty: An experimental verification study. Journal of biomechanics, 48(1), 59-64.

[10] Beckmann, J., Ferguson, S. J., Gebauer, M., Luering, C., Gasser, B., & Heini, P. (2007). Femoroplasty–augmentation of the proximal femur with a composite bone cement–feasibility, biomechanical properties and osteosynthesis potential. Medical engineering & physics, 29(7), 755-764.

[11] Beckmann, J., Springorum, R., Vettorazzi, E., Bachmeier, S., Lüring, C., Tingart, M., ... & Amling, M. (2011). Fracture prevention by femoroplasty—cement augmentation of the proximal femur. Journal of Orthopaedic Research,29(11), 1753-1758.

[12] Bevill, G., Farhamand, F., & Keaveny, T. M. (2009). Heterogeneity of yield strain in low-density versus high-density human trabecular bone. Journal of Biomechanics, 42(13), 2165-2170.

[13] Borau, C., Polacheck, W. J., Kamm, R. D., & García-Aznar, J. M. (2014). Probabilistic Voxel-Fe model for single cell motility in 3D. *In silico cell and tissue science*, *1*(1), 1-17.

[14] Bourne, B. C., & van der Meulen, M. C. (2004). Finite element models predict cancellous apparent modulus when tissue modulus is scaled from specimen CT-attenuation. Journal of biomechanics, 37(5), 613-621.

[15] Buehler, M. J. (2008). Nanomechanics of collagen fibrils under varying cross-link densities: atomistic and continuum studies. J. Mech. Behav. Biomed. Mater. 1, 59–67.

[16] Burr, D. B. (2016). The use of finite element analysis to estimate the changing strength of bone following treatment for osteoporosis. Osteoporosis International, 27(9), 2651-2654.

[17] Carter, D. R., & Hayes, W. C. (1977). The compressive behavior of bone as a two-phase porous structure. The Journal of Bone & Joint Surgery, 59(7), 954-962.

[18] Chen, J. H., Liu, C., You, L., & Simmons, C. A. (2010). Boning up on Wolff's Law: mechanical regulation of the cells that make and maintain bone. Journal of biomechanics, 43(1), 108-118.

[19] Chevalier, Y., Pahr, D., Allmer, H., Charlebois, M., & Zysset, P. (2007). Validation of a voxel-based FE method for prediction of the uniaxial apparent modulus of human trabecular bone using macroscopic mechanical tests and nanoindentation. Journal of biomechanics, 40(15), 3333-3340.

[20] Consensus development conference: diagnosis, prophylaxis, and treatment of osteoporosis. Am J Med. 1993 Jun;94(6):646–50.

[21] Cook, R. B., & Zioupos, P. (2009). The fracture toughness of cancellous bone.Journal of biomechanics, 42(13), 2054-2060.

[22] Delmas, P. D., Bjarnason, N. H., Mitlak, B. H., Ravoux, A. C., Shah, A. S., Huster, W. J., ... & Christiansen, C. (1997). Effects of raloxifene on bone mineral density, serum cholesterol concentrations, and uterine endometrium in postmenopausal women. New England Journal of Medicine, 337(23), 1641-1647.

[23] Dendorfer, S., Maier, H. J., Taylor, D., & Hammer, J. (2008). Anisotropy of the fatigue behaviour of cancellous bone. *Journal of biomechanics, 41*(3), 636-641.

[24] Dobson, C. A., Sisias, G., Phillips, R., Fagan, M. J., & Langton, C. M. (2006). Three dimensional stereolithography models of cancellous bone structures from μCT data: Testing and validation of finite element results. Proceedings of the Institution of Mechanical Engineers, Part H: Journal of Engineering in Medicine,220(3), 481-484.

[25] Elffors, L. (1998). Are osteoporotic fractures due to osteoporosis?. Aging Clinical and Experimental Research, 10(3), 191-204.

[26] Eswaran, S. K., Gupta, A., Adams, M. F., & Keaveny, T. M. (2006). Cortical and trabecular load sharing in the human vertebral body. Journal of Bone and Mineral Research, 21(2), 307-314.

[27] Ettinger, B. (1998). Alendronate use among 812 women: prevalence of gastrointestinal complaints, noncompliance with patient instructions, and discontinuation. Journal of Managed Care Pharmacy, 4(5), 488-492.

[28] Fliri, L., Sermon, A., Wähnert, D., Schmoelz, W., Blauth, M., & Windolf, M. (2013). Limited V-shaped cement augmentation of the proximal femur to prevent secondary hip fractures. Journal of biomaterials applications, 28(1), 136-143.

[29] Follet, H., Peyrin, F., Vidal-Salle, E., Bonnassie, A., Rumelhart, C., & Meunier, P. J. (2007). Intrinsic mechanical properties of trabecular calcaneus determined by finite-element models using 3D synchrotron microtomography. Journal of biomechanics, 40(10), 2174-2183.

[30] G. Boivin, P. J. Meunier. (2003). The mineralization of bone tissue: a forgotten dimension in osteoporosis research. Osteoporos Int (2003) 14 (Suppl 3): S19–S24

[31] Garijo, N., Manzano, R., Osta, R., & Perez, M. A. (2012). Stochastic cellular automata model of cell migration, proliferation and differentiation: Validation with in vitro cultures of muscle satellite cells. Journal of theoretical biology, 314, 1-9.

[32] Gibson, L. (1985). The mechanical behaviour of cancellous bone. Journal of biomechanics, 18(5), 317-328.

[33] Gibson, L. J., & Ashby, M. F. (1982, July). The mechanics of three-dimensional cellular materials. In Proceedings of the Royal Society of London A: Mathematical, Physical and Engineering Sciences (Vol. 382, No. 1782, pp. 43-59). The Royal Society.

[34] Gibson, L. J., & Ashby, M. F. (1999). Cellular solids: structure and properties. Cambridge university press.

[35] Gibson, L. J., Ashby, M. F., & Harley, B. A. (2010). Cellular materials in nature and medicine. Cambridge University Press.

[36] Gibson, L. J., Ashby, M. F., Schajer, G. S., & Robertson, C. I. (1982, July). The mechanics of two-dimensional cellular materials. In Proceedings of the Royal Society of London A: Mathematical, Physical and Engineering Sciences(Vol. 382, No. 1782, pp. 25-42). The Royal Society.

[37] Goff, M. G., Lambers, F. M., Sorna, R. M., Keaveny, T. M., & Hernandez, C. J. (2015). Finite element models predict the location of microdamage in cancellous bone following uniaxial loading. Journal of biomechanics, 48(15), 4142-4148.

[38] González, J., Riancho, J. (2004). Manual práctico de osteoporosis y enfermedades del metabolismo mineral. Madrid, España. Jarpyo Editores.

[39] Gupta HS, Zioupos P (2008) Fracture of bone tissue: The [‘]hows’ and the [‘]whys’. Med Eng Phys 30(10):1209–1226

[40] Hambli, R. (2013). Micro-CT finite element model and experimental validation of trabecular bone damage and fracture. Bone, 56(2), 363-374.

[41] Hamed, E., Jasiuk, I., Yoo, A., Lee, Y., & Liszka, T. (2012). Multi-scale modelling of elastic moduli of trabecular bone. Journal of The Royal Society Interface, rsif20110814.

[42] Harrison, N. M., McDonnell, P. F., O’Mahoney, D. C., Kennedy, O. D., O’Brien, F. J., & McHugh, P. E. (2008). Heterogeneous linear elastic trabecular bone modelling using micro-CT attenuation data and experimentally measured heterogeneous tissue properties. Journal of biomechanics, 41(11), 2589-2596.

[43] Harrison, N. M., McDonnell, P., Mullins, L., Wilson, N., O'Mahoney, D., & McHugh, P. E. (2013). Failure modelling of trabecular bone using a non-linear combined damage and fracture voxel finite element approach. Biomechanics and modeling in mechanobiology, 12(2), 225-241.

[44] Heini, P. F., Franz, T., Fankhauser, C., Gasser, B., & Ganz, R. (2004). Femoroplasty-augmentation of mechanical properties in the osteoporotic proximal femur: a biomechanical investigation of PMMA reinforcement in cadaver bones. Clinical Biomechanics, 19(5), 506-512.

[45] Jakob, F., Ebert, R., Ignatius, A., Matsushita, T., Watanabe, Y., Groll, J., & Walles, H. (2013). Bone tissue engineering in osteoporosis. Maturitas, 75(2), 118-124.

[46] Jefferiss, C. D., Lee, A. J. C., & Ling, R. S. M. (1975). Thermal aspects of self-curing polymethylmethacrylate. Bone & Joint Journal, 57(4), 511-518.

[47] Johnell, O., & Kanis, J. A. (2006). An estimate of the worldwide prevalence and disability associated with osteoporotic fractures. Osteoporosis international,17(12), 1726-1733.

[48] Kabel, J., Van Rietbergen, B., Odgaard, A., & Huiskes, R. (1999). Constitutive relationships of fabric, density, and elastic properties in cancellous bone architecture. Bone, 25(4), 481-486.

[49] Kanis J. on behalf of the World Health Organization Scientific Group. Assessment of osteoporosis at the primary health care level [Internet]. Sheffield, UK: WHO Scientific Group Technical Report; (2007). Available from;http://www.shef.ac.uk/FRAX/pdfs/WHO_Technical_ Report.pdf.

[50] Kanis, J. A., McCloskey, E. V., Johansson, H., Cooper, C., Rizzoli, R., & Reginster, J. Y. (2013). European guidance for the diagnosis and management of osteoporosis in postmenopausal women. Osteoporosis international, 24(1), 23-57.

[51] Kannus, P., Parkkari, J., Niemi, S., Pasanen, M., Palvanen, M., Järvinen, M., & Vuori, I. (2000). Prevention of hip fracture in elderly people with use of a hip protector. New England journal of medicine, 343(21), 1506-1513.

[52] Keaveny, T. M., Borchers, R. E., Gibson, L. J., & Hayes, W. C. (1993). Trabecular bone modulus and strength can depend on specimen geometry.Journal of Biomechanics, 26(8), 991-1000.

[53] Keller, T. S. (1994). Predicting the compressive mechanical behavior of bone.Journal of biomechanics, 27(9), 1159-1168.

[54] Khovidhunkit, W., & Shoback, D. M. (1999). Clinical effects of raloxifene hydrochloride in women. Annals of internal medicine, 130(5), 431-439.

[55] Kim, S. B., Kim, Y. J., Yoon, T. L., Park, S. A., Cho, I. H., Kim, E. J., ... & Shin, J. W. (2004). The characteristics of a hydroxyapatite–chitosan–PMMA bone cement. Biomaterials, 25(26), 5715-5723.

[56] Ladd, A.J.C., Kinney, J.H. (1998) Numerical errors and uncertainties in finite-element modeling of trabecular bone. Journal of Biomechanics 31, 941-945.

[57] Lane, J., Russell .L., Khan, S.,2000. Osteoporosis. Clin. Orthop. Relat. Res. 372, 139–150.

[58] Marks SC. Hermey DC. The structure and development of bone. In: Principles of bone biology. Bilezikian JB, Raize LG, Rodan GA (eds). New York, NY: Academic Press, 1996.

[59] Müller, R., & Rüegsegger, P. (1995). Three-dimensional finite element modelling of non-invasively assessed trabecular bone structures. Medical engineering & physics, 17(2), 126-133.

[60] O'Brien FJ, Taylor D, Lee TC (2002) An improved labelling technique for monitoring microcrack growth in compact bone. J Biomech 35((4):523–526

[61] Odén, A., McCloskey, E. V., Johansson, H., & Kanis, J. A. (2013). Assessing the impact of osteoporosis on the burden of hip fractures. Calcified tissue international, 92(1), 42-49.

[62] Olszta, M. J., Cheng, X. G., Jee, S. S., Kumar, R., Kim, Y. Y., Kaufman, M. J., Douglas, E. P. & Gower, L. B. (2007). Bone structure and formation: a new perspective. Mater. Sci. Eng. R 58, 77–116.

[63] Pace, A., Valenza, A., & Vitale, G. (2014). Mechanical characterization of human cancellous bone tissue by static compression tests. I materiali biocompatibili per la medicina/Biomaterials for Medicine: Atti del Convegno Nazionale della Società Italiana Biomateriali. Palermo, 2-4 luglio 2014, 15.

[64] Pahr, D. H., & Zysset, P. K. (2008). Influence of boundary conditions on computed apparent elastic properties of cancellous bone. Biomechanics and modeling in mechanobiology, 7(6), 463-476.

[65] Parkinson, I. H., Badiei, A., Stauber, M., Codrington, J., Müller, R., & Fazzalari, N. L. (2012). Vertebral body bone strength: the contribution of individual trabecular element morphology. Osteoporosis International, 23(7), 1957-1965.

[66] Pérez, M. A., & Prendergast, P. J. (2007). Random-walk models of cell dispersal included in mechanobiological simulations of tissue differentiation. Journal of biomechanics, 40(10), 2244-2253.

[67] Perilli, E., Baleani, M., Öhman, C., Fognani, R., Baruffaldi, F., & Viceconti, M. (2008). Dependence of mechanical compressive strength on local variations in microarchitecture in cancellous bone of proximal human femur. Journal of biomechanics, 41(2), 438-446.

[68] Pioletti, D. P. (2010). Biomechanics in bone tissue engineering. Computer methods in biomechanics and biomedical engineering, 13(6), 837-846.

[69] Polgar, K., Viceconti M, O'Connor, JJ. (2001) A comparison between automatically generated linear and parabolic tetrahedral when used to mesh a human femur. Proceedings of the Insitutition of Mechanical Engineers. Part H. Journal of engineering in medicine. 215(1), 85-94

[70] Rajan, K. (1985). Linear elastic properties of trabecular bone: a cellular solid approach. Journal of materials science letters, 4(5), 609-611.

[71] Ramos, A., & Simoes, J. A. (2006). Tetrahedral versus hexahedral finite elements in numerical modelling of the proximal femur. Medical engineering & physics, 28(9), 916-924.

[72] Riggs, B. L., & Melton, L. 3. (1995). The worldwide problem of osteoporosis: insights afforded by epidemiology. Bone, 17(5), S505-S511

[73] Rubin, C., Turner, A. S., Müller, R., Mittra, E., McLeod, K., Lin, W., & Qin, Y. X. (2002). Quantity and quality of trabecular bone in the femur are enhanced by a strongly anabolic, noninvasive mechanical intervention. *Journal of Bone and Mineral Research*, *17*(2), 349-357.

[74] Saito, E., Kang, H., Taboas, J. M., Diggs, A., Flanagan, C. L., & Hollister, S. J. (2010). Experimental and computational characterization of designed and fabricated 50: 50 PLGA porous scaffolds for human trabecular bone applications. Journal of Materials Science: Materials in Medicine, 21(8), 2371-2383.

[75] Shim, V., Josten, C., Anderson, I., & Boheme, J. (2012). *Use of polyurethane foam in orthopaedic biomechanical experimentation and simulation*. INTECH Open Access Publisher.

[76] Silva, B. C., Leslie, W. D., Resch, H., Lamy, O., Lesnyak, O., Binkley, N., ... & Bilezikian, J. P. (2014). Trabecular bone score: a noninvasive analytical method

based upon the DXA image. Journal of Bone and Mineral Research, 29(3), 518-530.

[77] Stauber, M., Nazarian, A., & Müller, R. (2014). Limitations of global morphometry in predicting trabecular bone failure. Journal of Bone and Mineral Research, 29(1), 134-141.

[78] Sutter, E. G., Mears, S. C., & Belkoff, S. M. (2010). A biomechanical evaluation of femoroplasty under simulated fall conditions. Journal of orthopaedic trauma, 24(2), 95.

[79] Svedbom, A., Hernlund, E., Ivergård, M., Compston, J., Cooper, C., Stenmark, J., ... & Kanis, J. A. (2013). Osteoporosis in the European Union: a compendium of country-specific reports. Archives of osteoporosis, 8(1-2), 1-218.

[80] Taylor D (2003) Fracture mechanics: how does bone break?. *NatMater 2(3):133–134*

[81] Thompson, M. S., McCarthy, I. D., Lidgren, L., & Ryd, L. (2003). Compressive and shear properties of commercially available polyurethane foams. *Journal of biomechanical engineering*, *125*(5), 732-734.

[82] Turner, C. H., Cowin, S. C., Rho, J. Y., Ashman, R. B., & Rice, J. C. (1990). The fabric dependence of the orthotropic elastic constants of cancellous bone.Journal of biomechanics, 23(6), 549-561.

[83] Ulrich, D., van Rietbergen, B., Weinans, H., & Rüegsegger, P. (1998). Finite element analysis of trabecular bone structure: a comparison of image-based meshing techniques. Journal of biomechanics, 31(12), 1187-1192.

[84] Van Lenthe, G. H., Stauber, M., & Müller, R. (2006). Specimen-specific beam models for fast and accurate prediction of human trabecular bone mechanical properties. Bone, 39(6), 1182-1189.

[85] Van Rietbergen B, Weinans H, Huiskes R, Odgaard A. (1995). A new method to determine trabecular bone elastic properties and loading using micromechanical finite-element models. Journal of Biomechanics, 28(1), 69-81.

[86] Wachtel EF, Keaveny TM (1997) Dependence of trabecular damage on mechanical strain. J Orthop Res 15(5):781–787

[87] Wang, J., Zhou, B., Liu, X. S., Fields, A. J., Sanyal, A., Shi, X., ... & Guo, X. E. (2015). Trabecular plates and rods determine elastic modulus and yield strength of human trabecular bone. Bone, 72, 71-80.

[88] Yeh OC, Keaveny TM (2001) Relative roles of microdamage and microfracture in the mechanical behavior of trabecular bone. J Orthop Res 19(6):1001–1007

[89] Zysset, P. K. (2003). A review of morphology–elasticity relationships in human trabecular bone: theories and experiments. Journal of biomechanics, 36(10), 1469-1485.